Molecular Plant, Volume *14*

Supplemental information

A single-cell morpho-transcriptomic map of brassinosteroid action in the *Arabidopsis* root

Moritz Graeff, Surbhi Rana, Jos R. Wendrich, Julien Dorier, Thomas Eekhout, Ana Cecilia Aliaga Fandino, Nicolas Guex, George W. Bassel, Bert De Rybel, and Christian S. Hardtke

GRAEFF ET AL., SUPPLEMENTAL INFORMATION

Supplemental Figures S1-S20

Supplemental Methods S1: Creation of standardized, simplified root models.

Additional supplementary files:

Table S1: Differentially expressed genes in the scRNAseq data in stage-specific subclusters, *bri*^{TRIPLE} versus wild type comparison.

Table S2: Differentially expressed genes in the scRNAseq data in stage-specific subclusters, *bri*$^{T\text{-}RESCUE}$ versus wild type comparison.

Table S3: Differentially expressed genes in the scRNAseq data in stage-specific subclusters, *bri*$^{T\text{-}RESCUE}$ versus *bri*^{TRIPLE} comparison.

Table S4: Differentially expressed genes in the scRNAseq data in cell type-specific clusters.

Table S5: Comparison of the scRNAseq data with negatively brassinosteroid-responsive genes in the root.

Table S6: Comparison of the scRNAseq data with positively brassinosteroid-responsive genes in the root.

Table S7: Differential expression of arabinogalactans in scRNAseq clusters.

Table S8: Differential expression of expansins in scRNAseq clusters.

Movie S1: 3D reconstruction of a mature wild type root segment.

Movie S2: 3D reconstruction of a mature *bri*^{TRIPLE} root segment.

Movie S3: 3D reconstruction of a mature *bri*$^{T\text{-}RESCUE}$ root segment.

Movie S4: 3D reconstruction of a mature wild type root meristem.

Movie S5: 3D reconstruction of a mature *bri*^{TRIPLE} root meristem.

Movie S6: 3D reconstruction of a mature *bri*$^{T\text{-}RESCUE}$ root meristem.

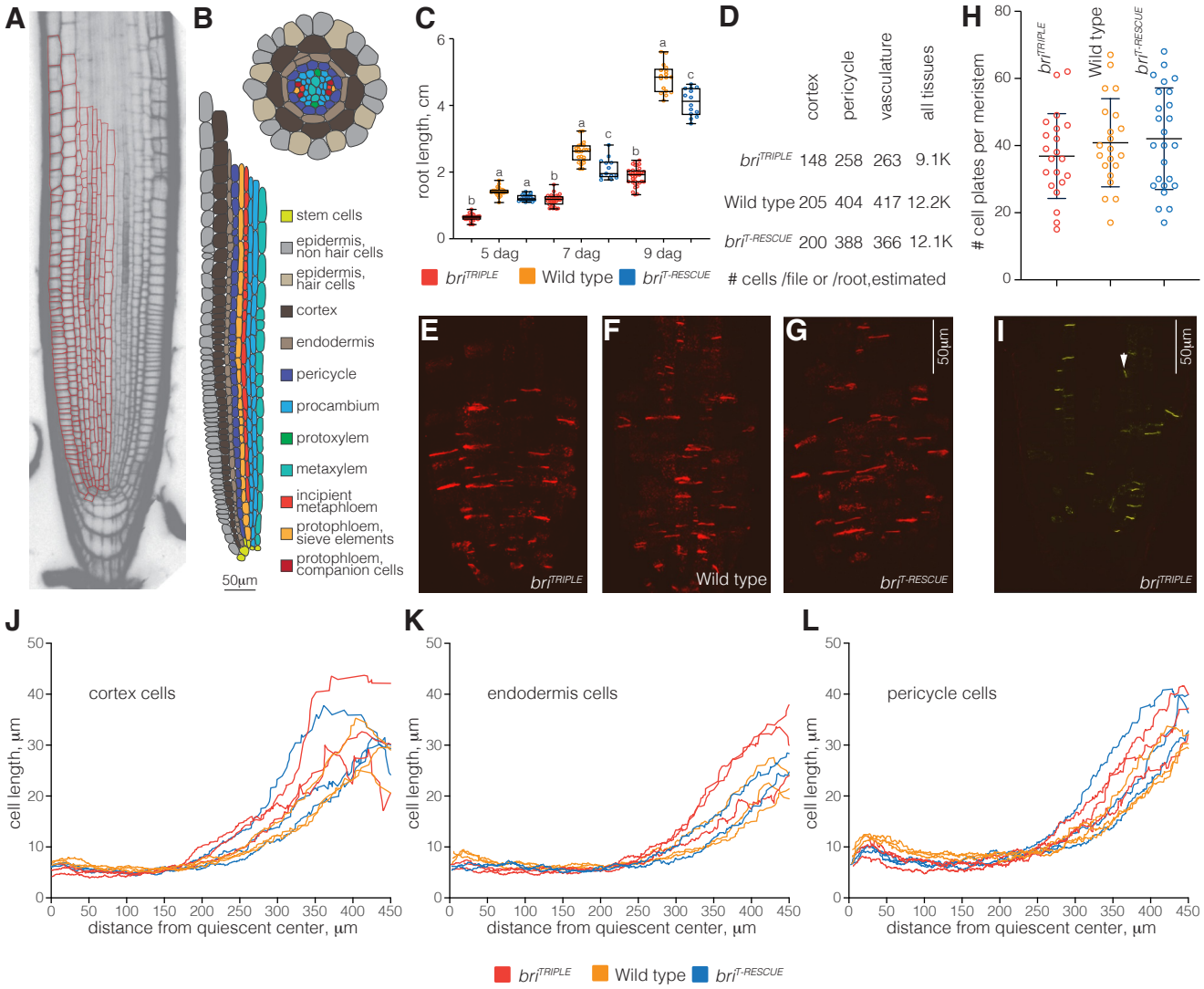

Figure S1 Schematic presentation of Arabidopsis root meristem organization, quantification of cell proliferation and root growth variability
(A) Transversal confocal section through the center of a representative 7-day-old Arabidopsis root meristem, oriented from phloem pole to phloem pole, merged with cell outlines (red) for one half. (B) Schematic presentation of the tissues in the root shown in (A), labeled for cell types, and a corresponding schematic of their radial arrangement. (C) Primary root length of indicated genotypes at 5, 7 and 9 days after germination (dag). Box plots display 2nd and 3rd quartiles and the median, bars indicate maximum and minimum. Statistical significance was determined by ordinary one-way ANOVA. Statistically significant different groups are indicated by different lowercase letters. (D) Estimated number of cells per cell file of indicated tissue or total root mature root cell number, calculated from the average root length (C) and the average cell lengths obtained for mature cells or average cell number per mature segment (Figure 1B). (E-G) Confocal microscopy images of root meristems from indicated genotypes, stained with anti-KN antibody (red fluorescence), showing the maximum projection of the 3D stacks from an entire meristem each. Cell plates of dividing cells are recognizable as sharp KN signal accumulations. (H) Dividing cells per meristem as deduced from cell plates detected by anti-KN immunostaining. Bars indicate the mean and standard deviation. Differences between genotypes were not significant (one-way ANOVA). (I) As in E-G, for a single slice from a 3D stack. The arrowhead points out a late periclinal division. (J-L) Cell length as a function of distance from the QC, for cortex (J), endodermis (K) and pericycle (L) cell files for a few selected individual roots, obtained through the *PlantSeg-MorphoGraphX-3DCellAtlas* pipeline. Note the substantial variability within and between genotypes.

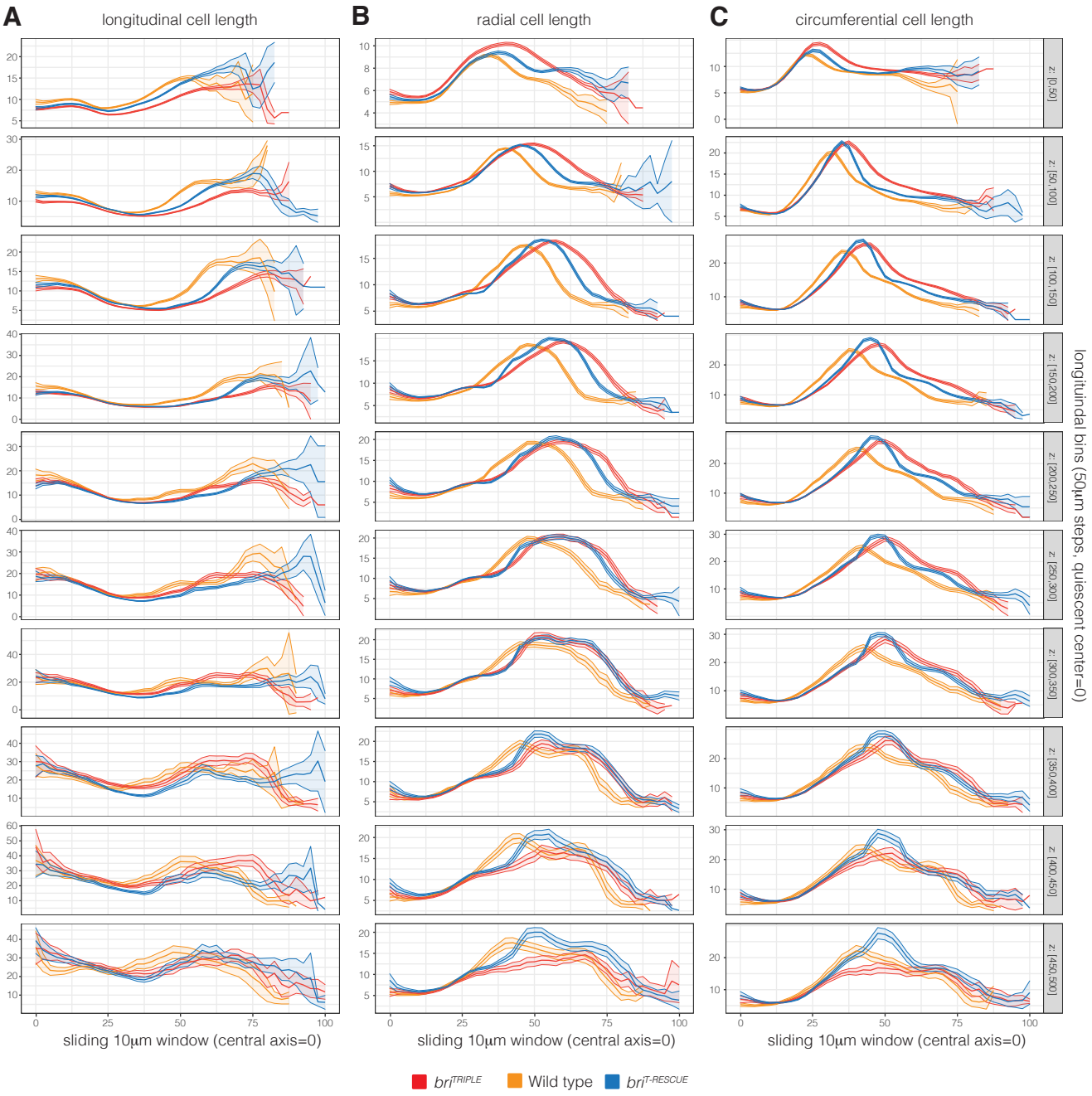

Figure S2 Comparative radial sliding window analysis of standardized root models 1 Quantitative features of each simplified root meristem model using concentric 10 µm thick and 50 µm high cylindrical shells with increasing radius (x-axis) fixed z-position (indicated on the right). Average parameters were calculated by taking into account cells whose centers fell into the corresponding shell. The graphs indicate average longitudinal cell length (µm) (A), cell width in the radial dimension (µm) (B) and cell width in the circumferential dimension (µm) (C) for 11-12 roots per genotype combined. The shaded regions indicate +/- standard error of the mean. Note the displacement of the *bri*^{TRIPLE} measurements as compared to wild type on the x axes, due to the increased diameter of *bri*^{TRIPLE} meristems.

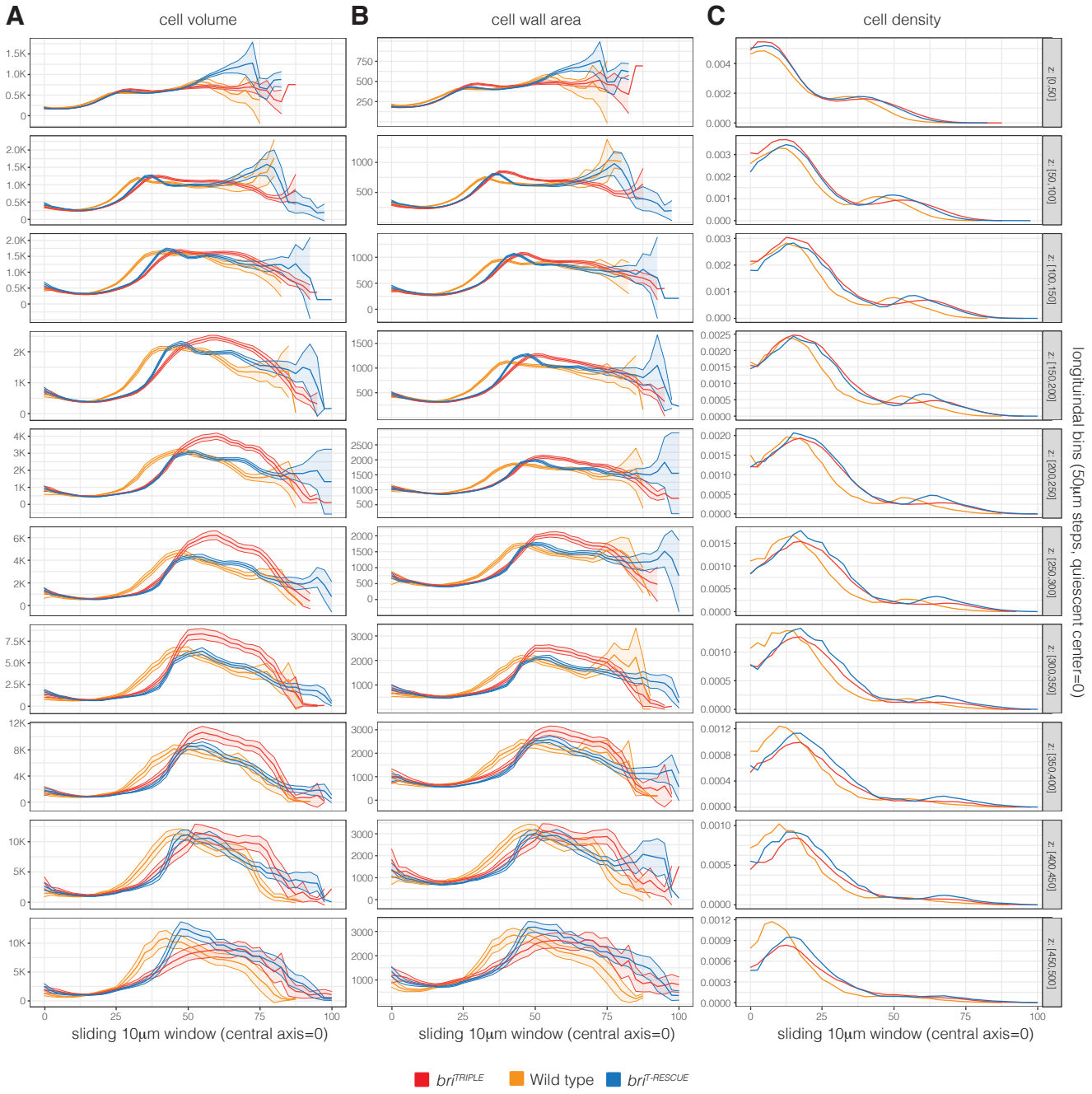

Figure S3 Comparative radial sliding window analysis of standardized root models 2 Continuation of the analysis presented in Figure S2, indicating cell volume (µm³) (A), cell wall area (µm²) (B), and cell density (cells/µm³) (C) for 11-12 roots per genotype combined. The +/- standard error of the mean is indicated where applicable. Note the displacement of the *bri*^{TRIPLE} measurements as compared to wild type on the x axes, due to the increased diameter of *bri*^{TRIPLE} meristems.

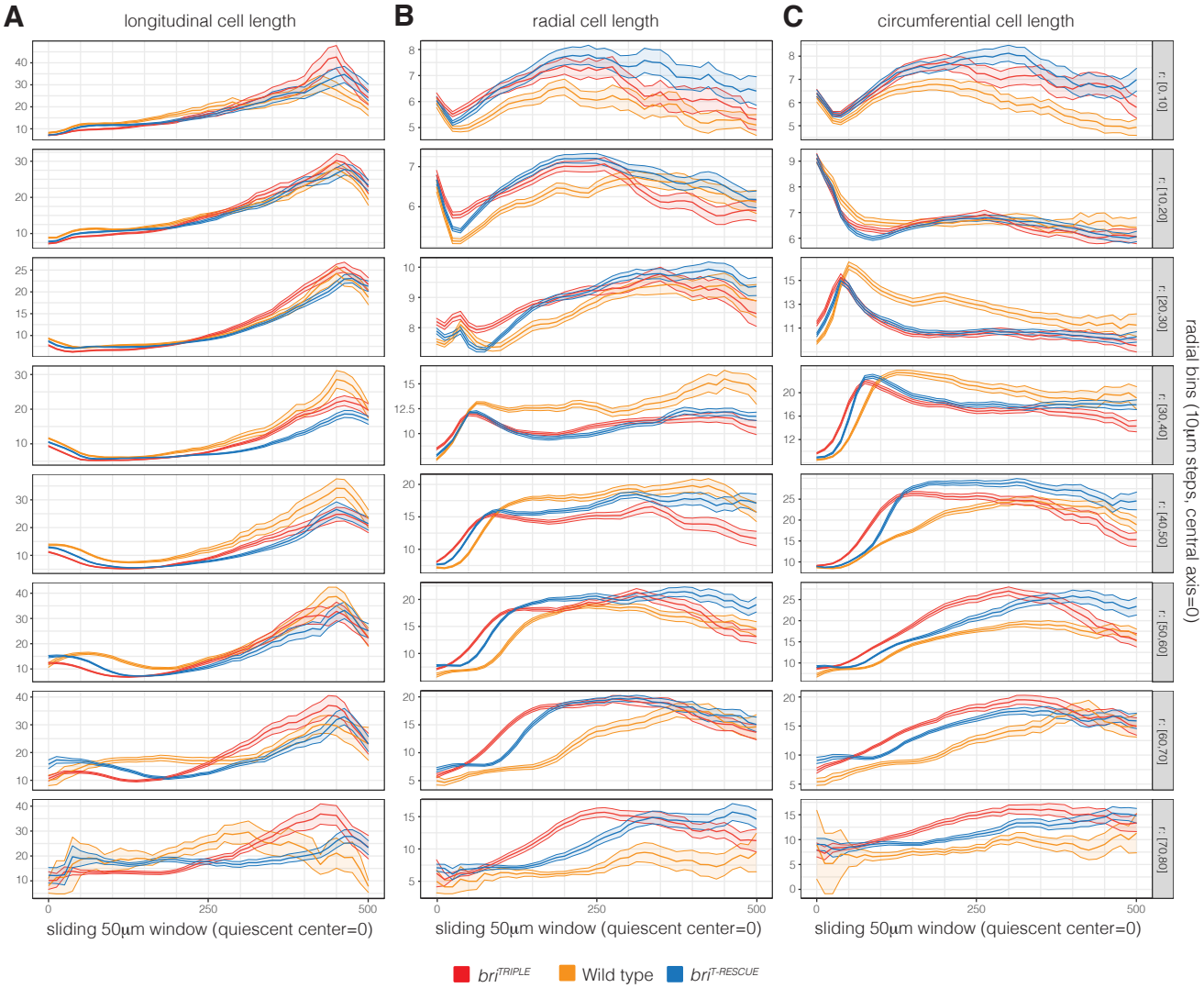

Figure S4 Comparative longitudinal sliding window analysis of standardized root models 1 Sliding window analysis similar to Figure S2, for a 10 µm thick and 50 µm high cylindrical shell (centered on the z-axis) with fixed radius (indicated on the right) and z-position sliding from the QC to the elongation-differentiation zone (x-axis). The graphs indicate average longitudinal cell length (µm) (A), cell width in the radial dimension (µm) (B) and cell width in the circumferential dimension (µm) (C) for 11-12 roots per genotype combined. Shaded regions indicate the +/- standard error of the mean. Note that curves within single panels are not always representing similar tissues, because of the wider stele of *bri*^{TRIPLE} meristems.

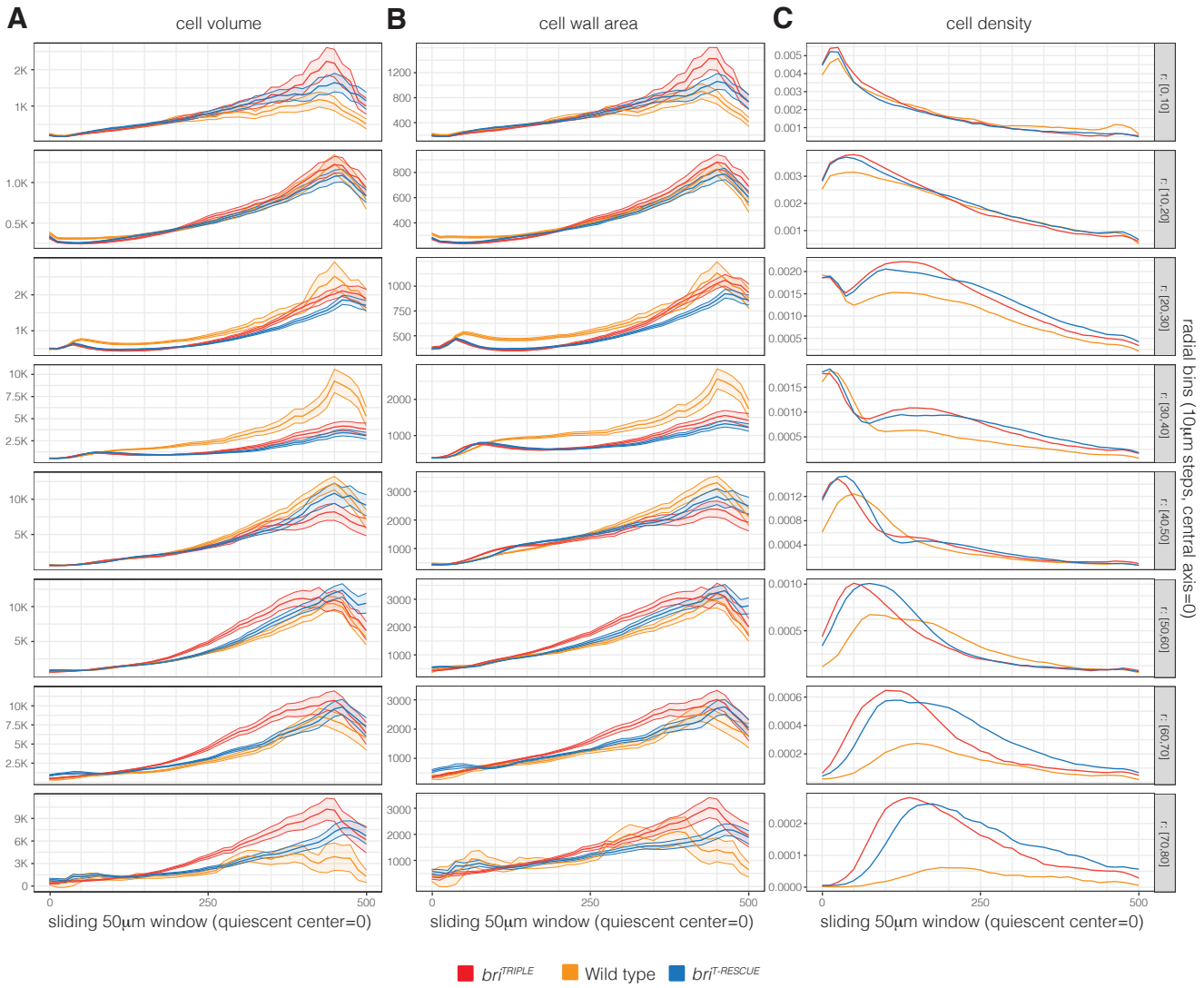

Figure S5 Comparative longitudinal sliding window analysis of standardized root models 2 Continuation of the analysis presented in Figure S4, indicating cell volume (µm^3) (A), cell wall area (µm^2) (B), and cell density (C) for 11-12 roots per genotype combined. Shaded regions indicate the +/- standard error of the mean where applicable. Note that curves within single panels are not always representing similar tissues, because of the wider stele of *bri*^{TRIPLE} meristems.

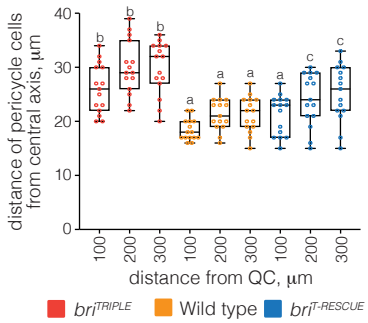

Figure S6 Stele width in wild-type, *bri*^{TRIPLE} and *bri*$^{T\text{-}RESCUE}$ root meristems Average distance of pericycle cells from the central axis, for selected distances from the QC. Box plots display 2nd and 3rd quartiles and the median, bars indicate maximum and minimum. Statistical significance was determined by ordinary one-way ANOVA. Statistically significant different groups are indicated by different lowercase letters.

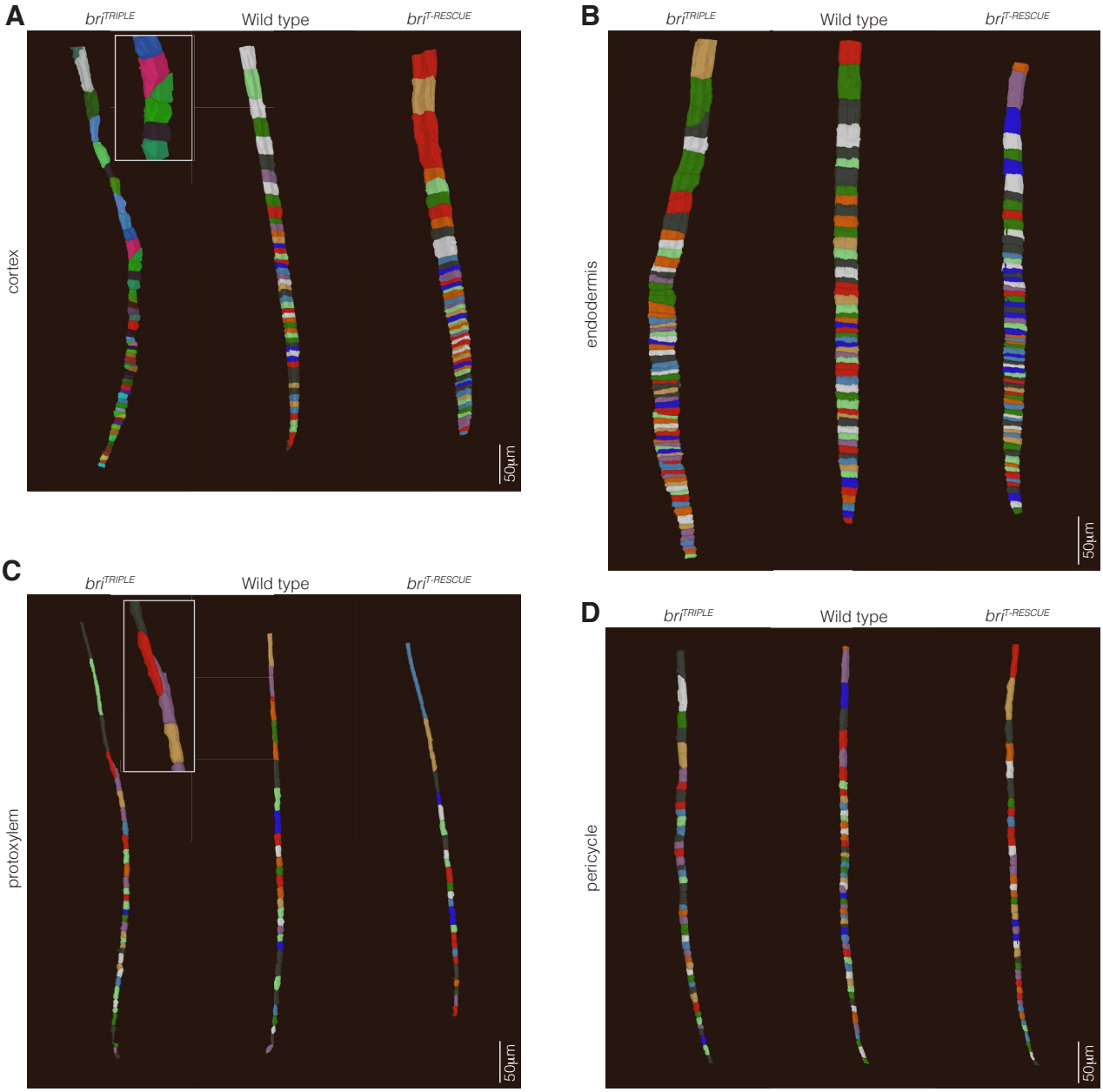

Figure S7 Examples of cell files in wild-type, *bri*^{TRIPLE} and *bri*$^{T\text{-}RESCUE}$ root meristems (A-D) Examples of isolated cell files for cortex (A), endodermis (B), protoxylem (C), and pericycle (D), obtained from segmentations via the *PlantSeg-MorphoGraphX-3DCellAtlas* pipeline. Note the frequently oblique cell division planes in *bri*^{TRIPLE} mutants and the “ballooning effect”, highlighted by inlays.

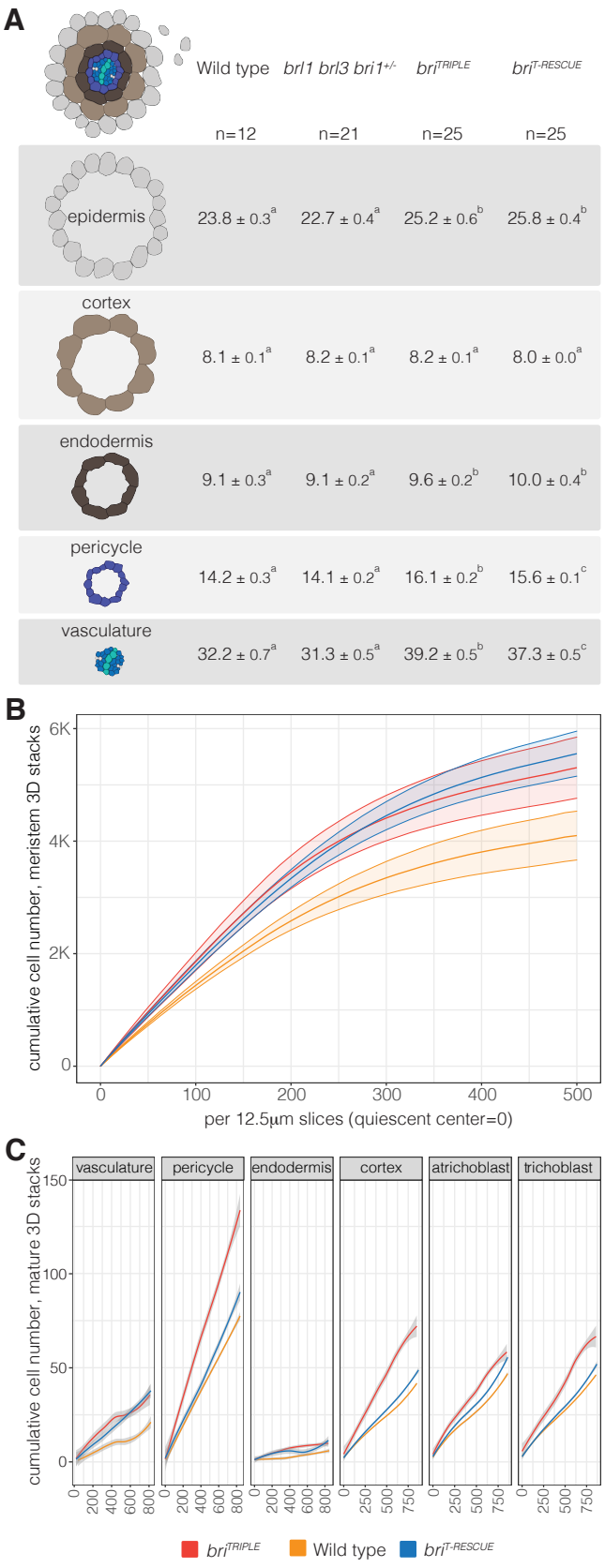

Figure S8 Quantification of cell files in wild-type, *bri*^{TRIPLE} and *bri*$^{T\text{-}RESCUE}$ roots (A) Quantification of cell file numbers in the different root tissues, obtained from histological cross sections taken at the level of differentiated protoxylem. Statistically significantly different groups are indicated by lower case letters. (B) Cumulative cell file number in root meristems, counted in 12.5 µm slices from the QC to the elongation-differentiation zone, with +/- standard error of the mean. (C) Cumulative cell number in mature root area segmentation spanning 800 µm in length and starting ~1 cm above the root meristem, with +/- standard error of the mean.

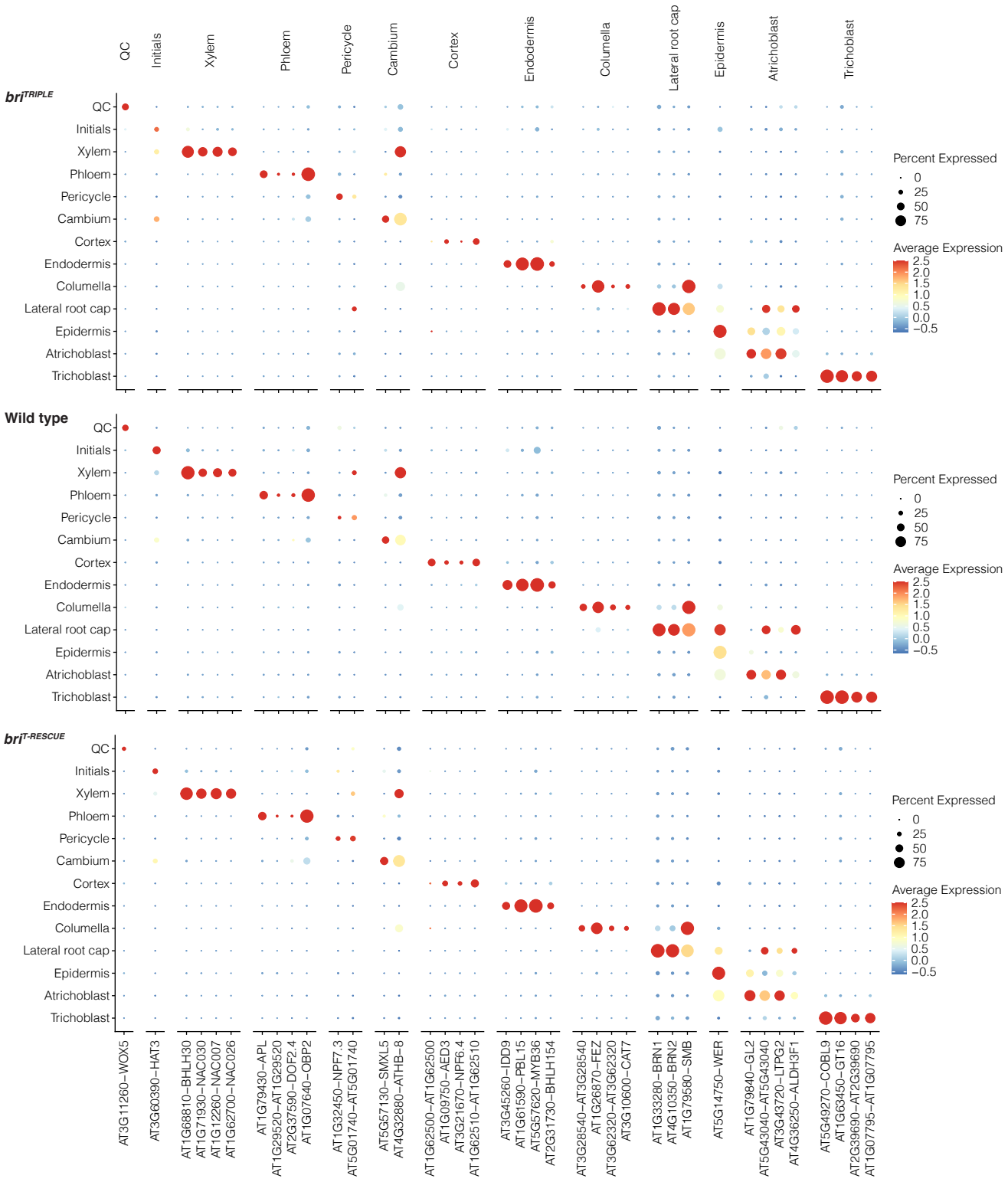

Figure S9 Assignment of cell identities Expression of known cell-type marker genes across cells for the three different genotypes. Dot diameter indicates the proportion of cluster cells expressing a given gene, color indicates the mean expression across cells in a cluster.

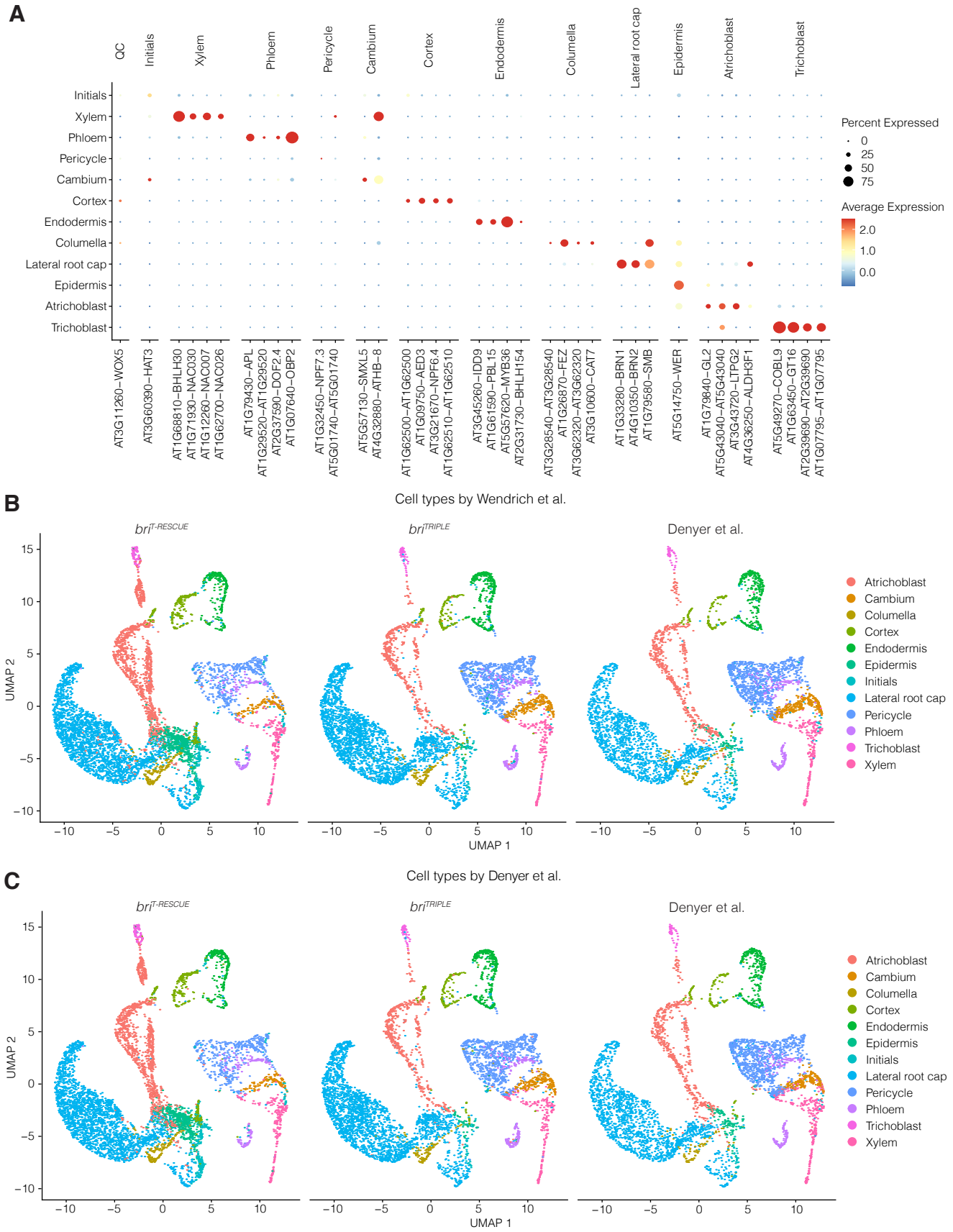

Figure S10 Comparison of scRNAseq cell type clusters with an outside reference data set (A) Dot plot of validated marker genes confirms identity of each annotated cell type cluster. Dot diameter indicates proportion of cells within the cluster that express the given gene; dot color indicates average expression value across the cells within the cluster. (B) Uniform Manifold Approximation and Projection (UMAP) of *bri*$^{T\text{-}RESCUE}$, *bri*^{TRIPLE} and the Denyer et al. 2019 reference dataset, with cell type annotations based on the Wendrich et al. 2020 dataset. (C) UMAP of *bri*$^{T\text{-}RESCUE}$, *bri*^{TRIPLE} and the Denyer et al. 2019 reference dataset, with cell type annotations based on the Denyer et al. 2019 dataset.

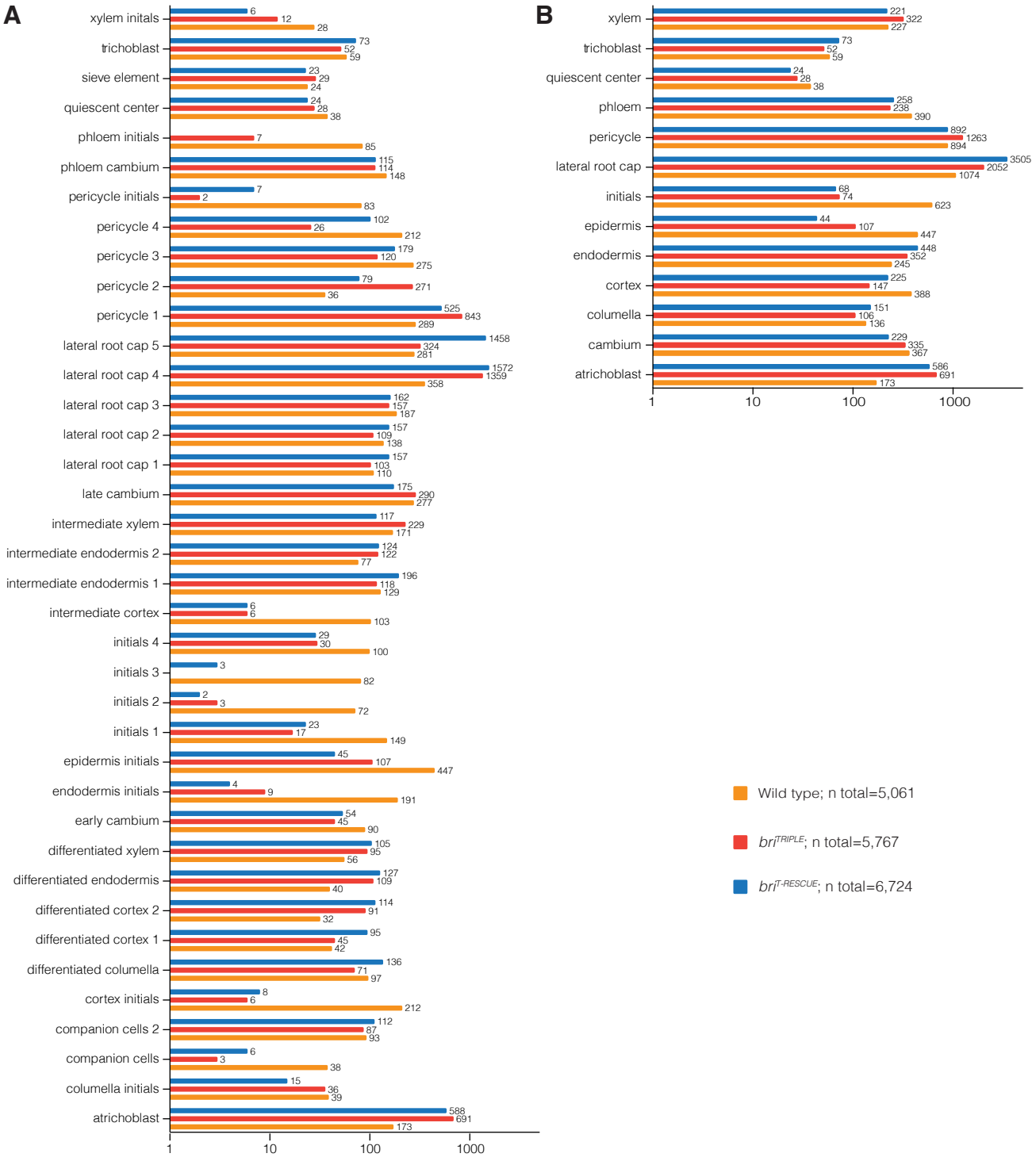

Figure S11 Cell type abundance in the scRNAseq datasets (A) Absolute cell numbers per cluster in wild-type, *bri*^{TRIPLE}, and *bri*$^{T\text{-}RESCUE}$ root meristem single cell transcriptomes, based on identity assignment with cell type-specific and stage-specific marker genes (Wendrich et al., 2020) (see Tables S1-S3). (B) As in (A), for the 13 principal cell types (see Table S4).

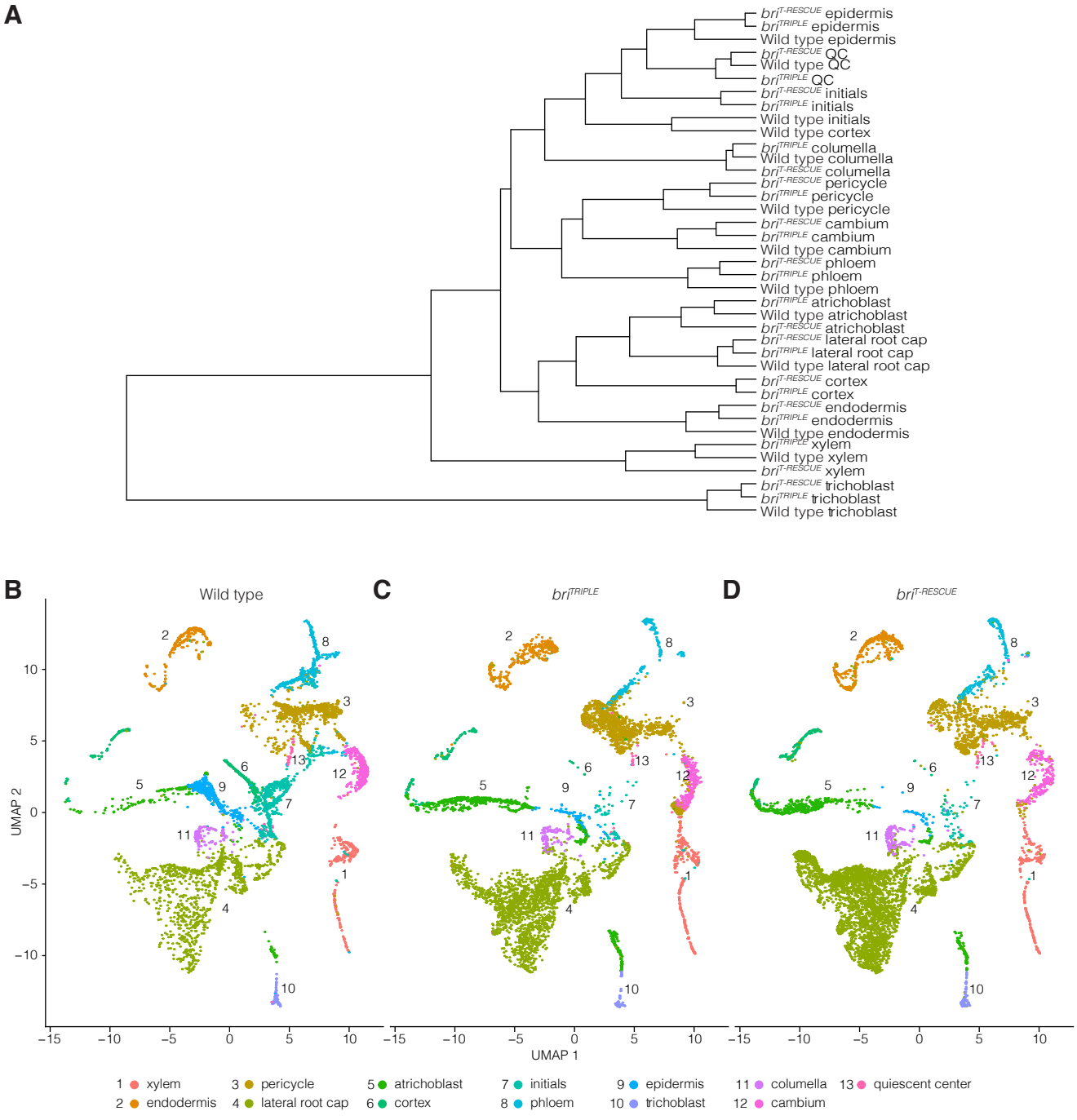

Figure S12 Dendrogram of identified cell types in all samples and overview of scRNAseq cell type clusters (A) Phylogenetic tree relating the average cell from each cell type in each sample. The tree is estimated based on a distance matrix constructed using the first 20 principal components of the Seurat object. (B-D) Uniform Manifold Approximation and Projection (UMAP) of wild-type (B), *bri*^{TRIPLE} (C), and *bri*$^{T\text{-}RESCUE}$ (D) single cell transcriptomes, clustered based on assigned principal cell identities established by cell type-specific marker genes (Wendrich et al., 2020).

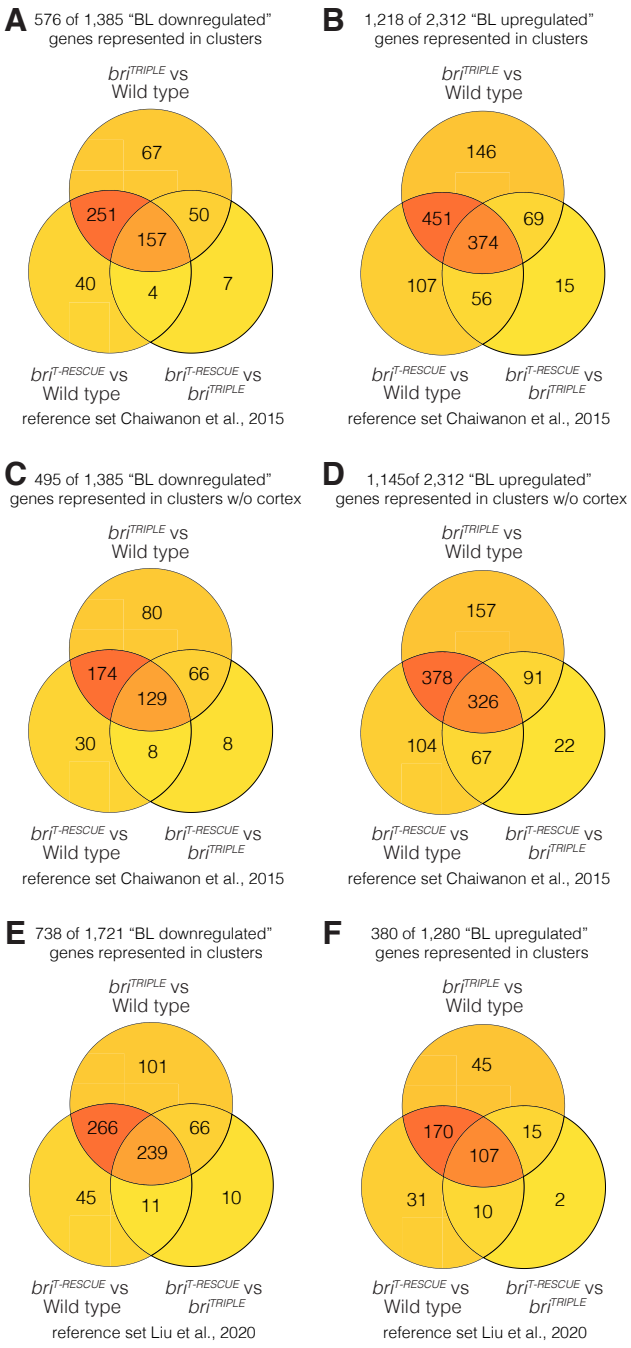

Figure S13 Comparison of scRNAseq data with known brassinosteroid-responsive genes (A-B) Venn diagram illustrating the overlap between genes that were differentially expressed between genotypes in the scRNA-seq dataset, and genes that were found to be downregulated (A) or upregulated (B) in response to brassinolide treatment in the root (Chaiwanon and Wang, 2015) (see also Table S5 and Table S6). (C-D) As in (A-B), but with the cortex cells removed from the scRNA-seq dataset. (E-F) As in (A-B), for a different reference set of genes that are considered high confidence brassinosteroid-downregulated (E) or upregulated (F) (Liu et al., 2020).

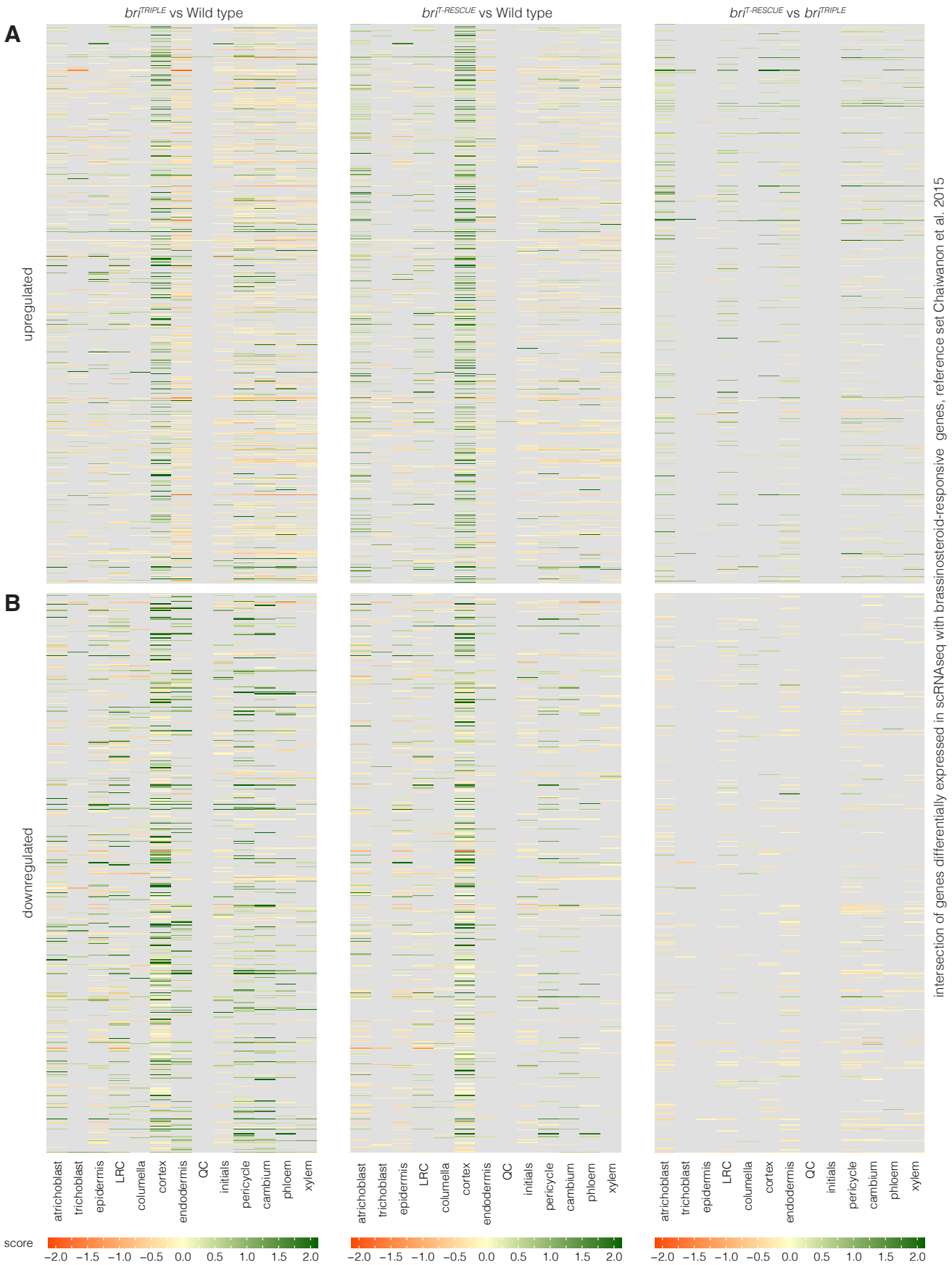

Figure S14 Brassinosteroid response in the scRNAseq profiles (A-B) Heatmap representing the expression of genes that were found to be upregulated (A) or downregulated (B) in response to brassinolide treatment in the root (Chaiwanon and Wang, 2015). The scRNA-seq dataset (Table S4) comprised 576 of 1,385 downregulated (Table S5) and 1,218 of 2,312 upregulated (Table S6) genes. Color scales with a fixed range from -2 to 2 indicate the expression score (logFC x percentage of cells expressing gene in cluster X in genotype a / percentage of cells expressing gene in cluster X in genotype b). Genes that were not detected in the cluster or had an adjusted *p* value >0.05 are displayed in grey.

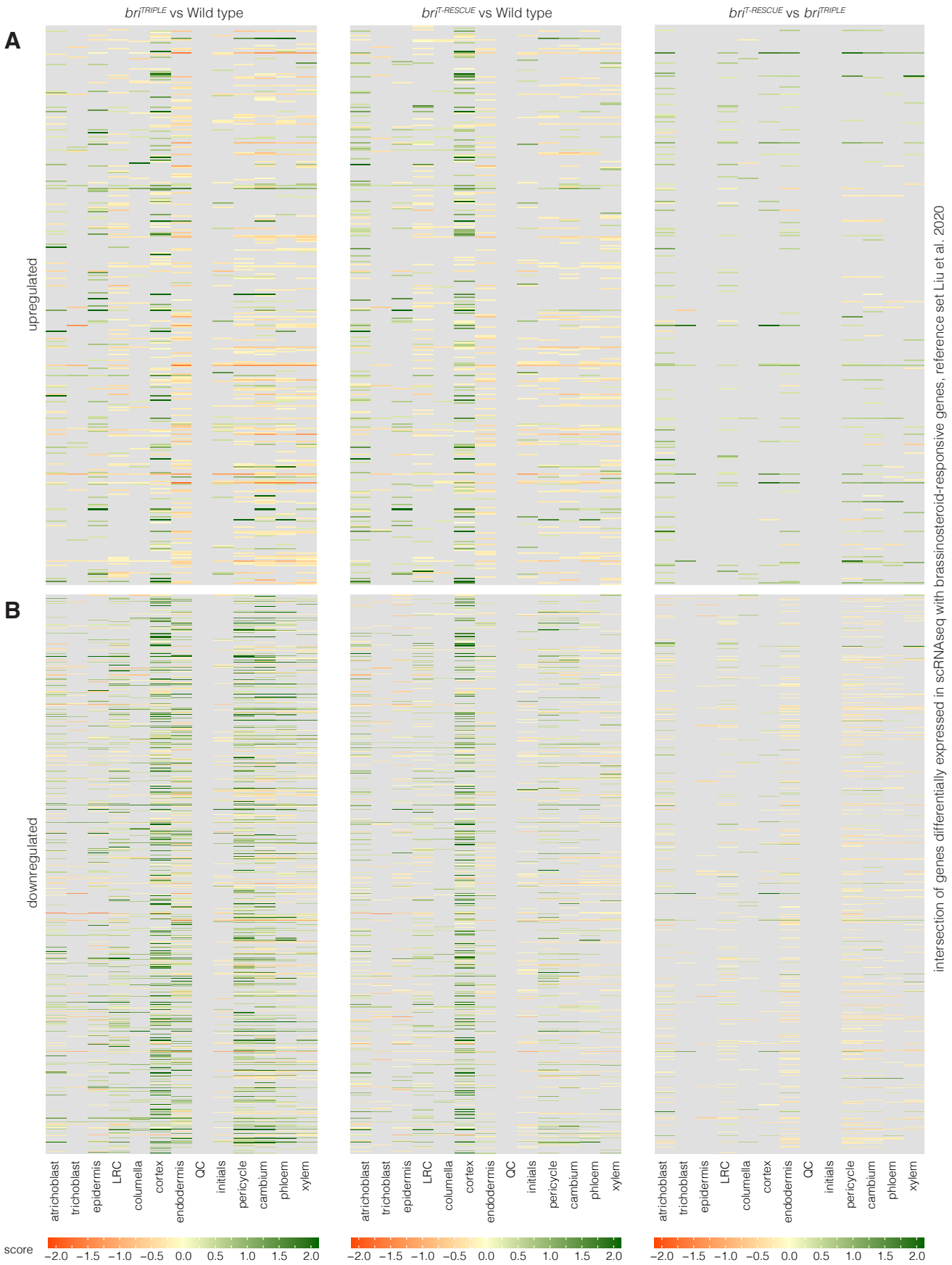

Figure S15 Brassinosteroid response in the scRNAseq profiles (A-B) Heatmap representing the expression of genes that are considered high confidence brassinosteroid-upregulated (A) or downregulated (B) (Liu et al., 2020). The scRNA-seq dataset comprised 380 of 1,280 upregulated and 738 of 1,721 downregulated genes. Color scales with a fixed range from -2 to 2 indicate the expression score (logFC x percentage of cells expressing gene in cluster X in genotype a / percentage of cells expressing gene in cluster X in genotype b). Genes that were not detected in the cluster or had an adjusted *p* value >0.05 are displayed in grey.

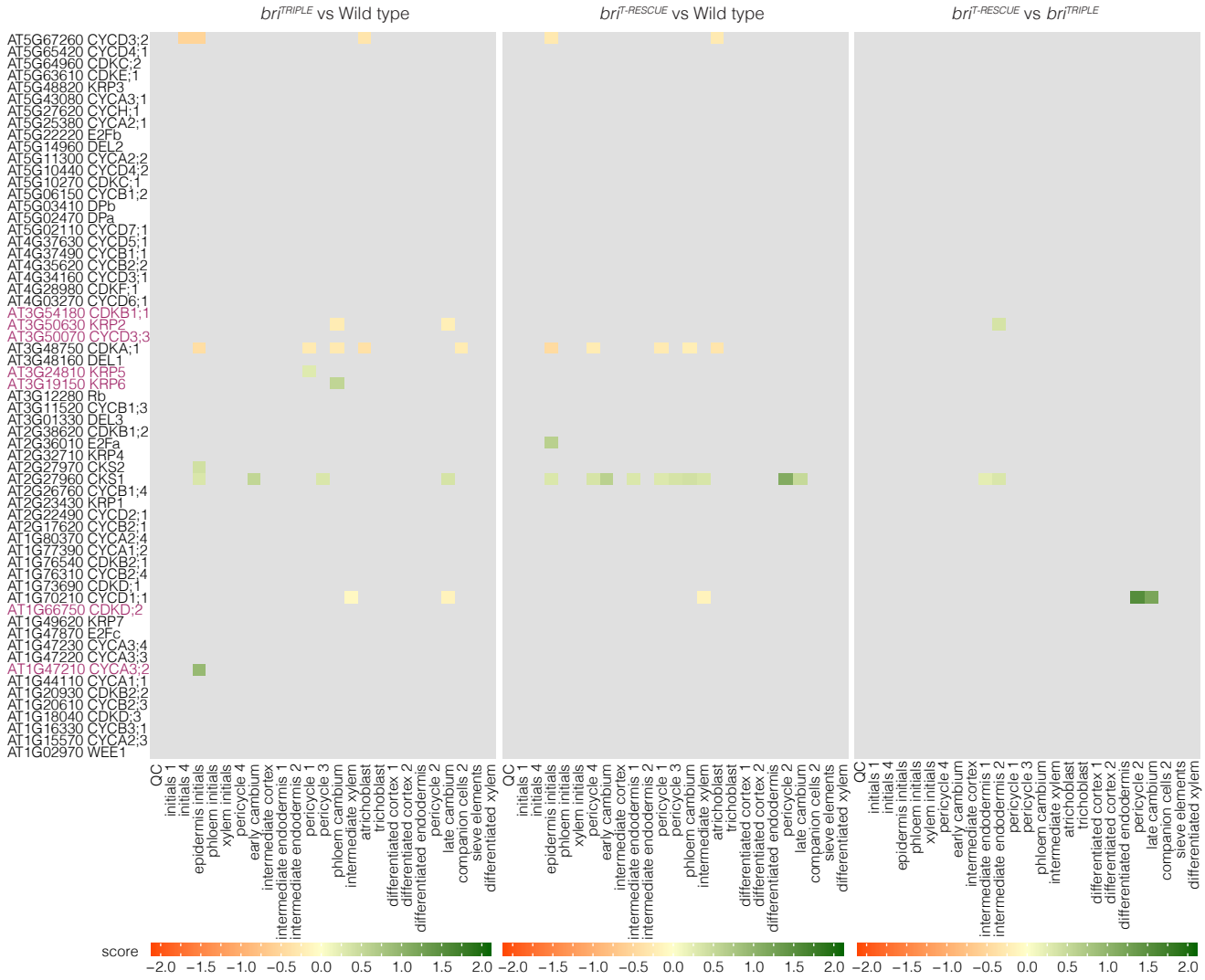

Figure S16 Core cell cycle marker gene expression Heatmap indicating the differential gene expression score of core cell cycle marker genes (Vandepoele et al., 2002) in scRNAseq subclusters and ordered with respect to stage-specific markers in increasing distance from the QC. Known brassinosteroid-responsive gene family members (Chaiwanon and Wang, 2015) are highlighted in purple.

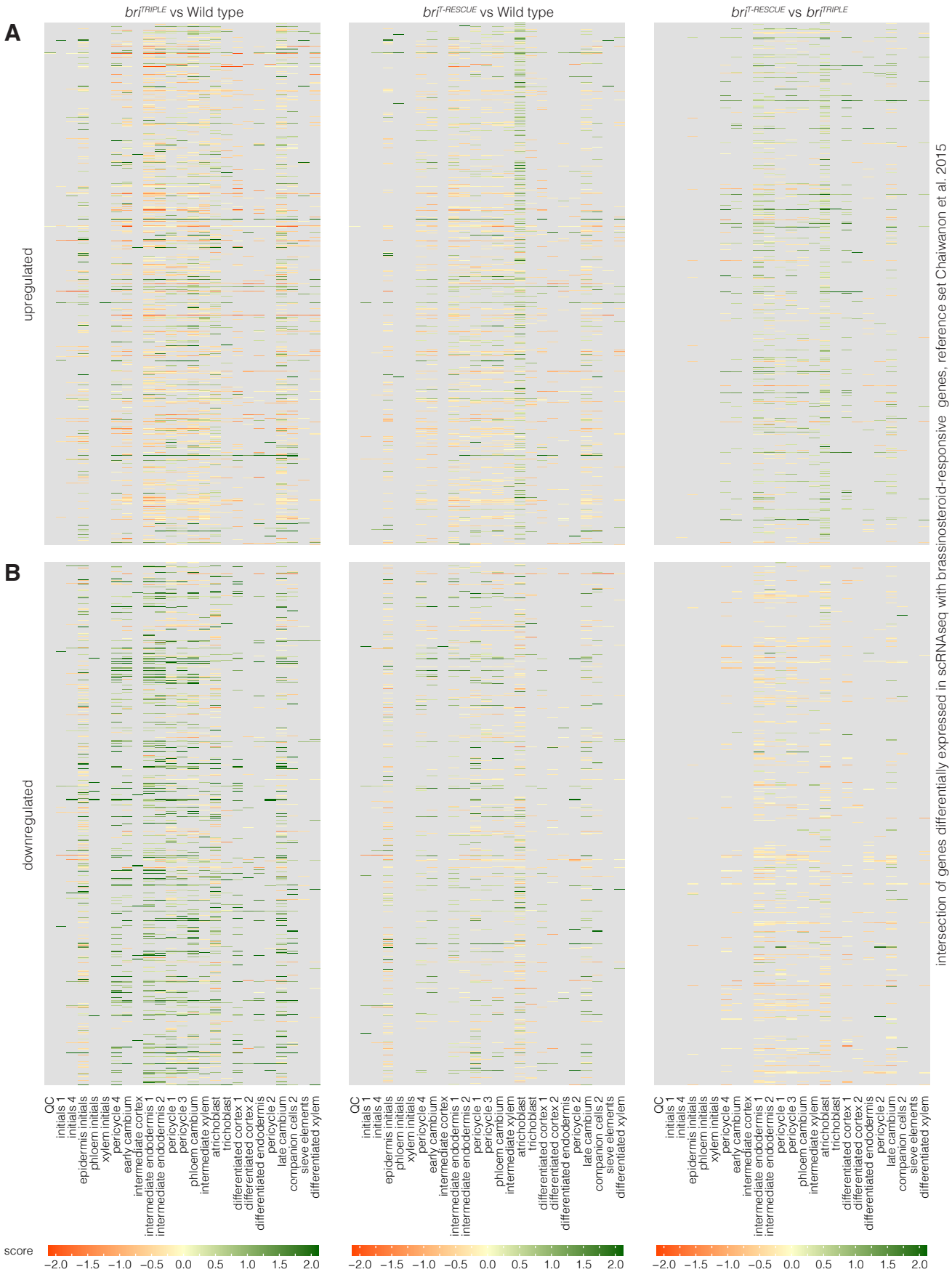

Figure S17 Spatial distribution of brassinosteroid response in the scRNAseq profiles (A) Heatmap representing the expression of genes that were found to be upregulated (A) or downregulated (B) in response to brassinolide treatment in the root (Chaiwanon and Wang, 2015), similar to Figure S14, but for subclusters and ordered with respect to stage-specific markers in increasing distance from the QC.

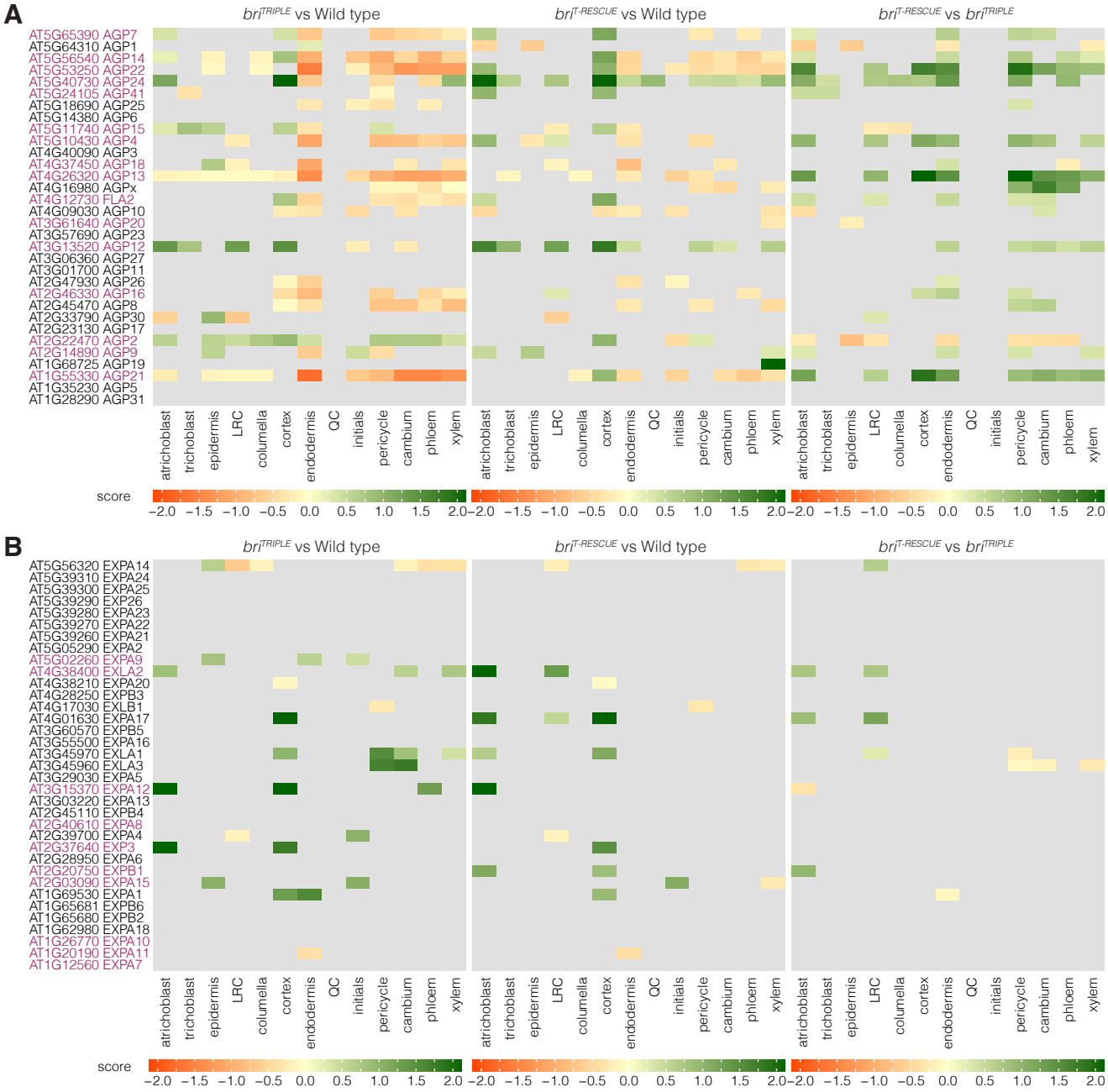

Figure S18 *AGP* gene expression in the scRNAseq profiles (A) Heatmap indicating the gene expression score of the 32 arabinogalactan proteins or peptides (AGPs) in the 13 general cell types. Note that AGPs show a consistent downregulation in the stele tissues and frequently also in ground tissues of *bri*^{TRIPLE} meristems, which is largely normalized in *bri*$^{T\text{-}RESCUE}$ meristems. (B) Expansins are a gene family of comparable size to AGPs (35 genes in *Arabidopsis*) and are associated with cell expansion. Note that compared to AGPs, their expression is affected less frequently and expression profiles are more varied between the different genotypes.

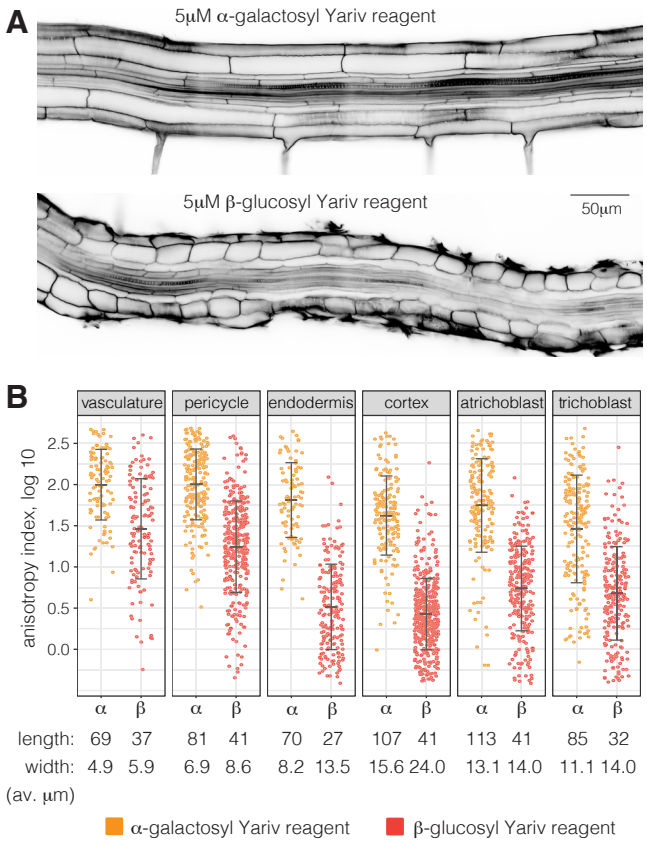

Figure S19 Quantification of cellular parameters upon AGP perturbation (A) Confocal sections of representative wild-type primary roots, ~1 cm above the root meristem, 4 days after transfer of 3-day-old seedlings on media containing α-galactosyl (control treatment) or β-glucosyl (a specific AGP inhibitor) Yariv reagents, illustrating reduced anisotropy of mature cells upon exposure to β-glucosyl Yariv reagent. (B) Quantitative comparison of cellular anisotropy in roots treated with α-galactosyl or β-glucosyl Yariv reagent, obtained by processing of 3D stacks with the *PlantSeg-MorphoGraphX-3DCellAtlas* pipeline and expressed as anisotropy index [longitudinal cell length ^ 2 / (radial cell length * circumferential cell length]. Whiskers indicate mean and standard deviation. Differences between treatments were statistically significant for all tissues ($p<0.001$).

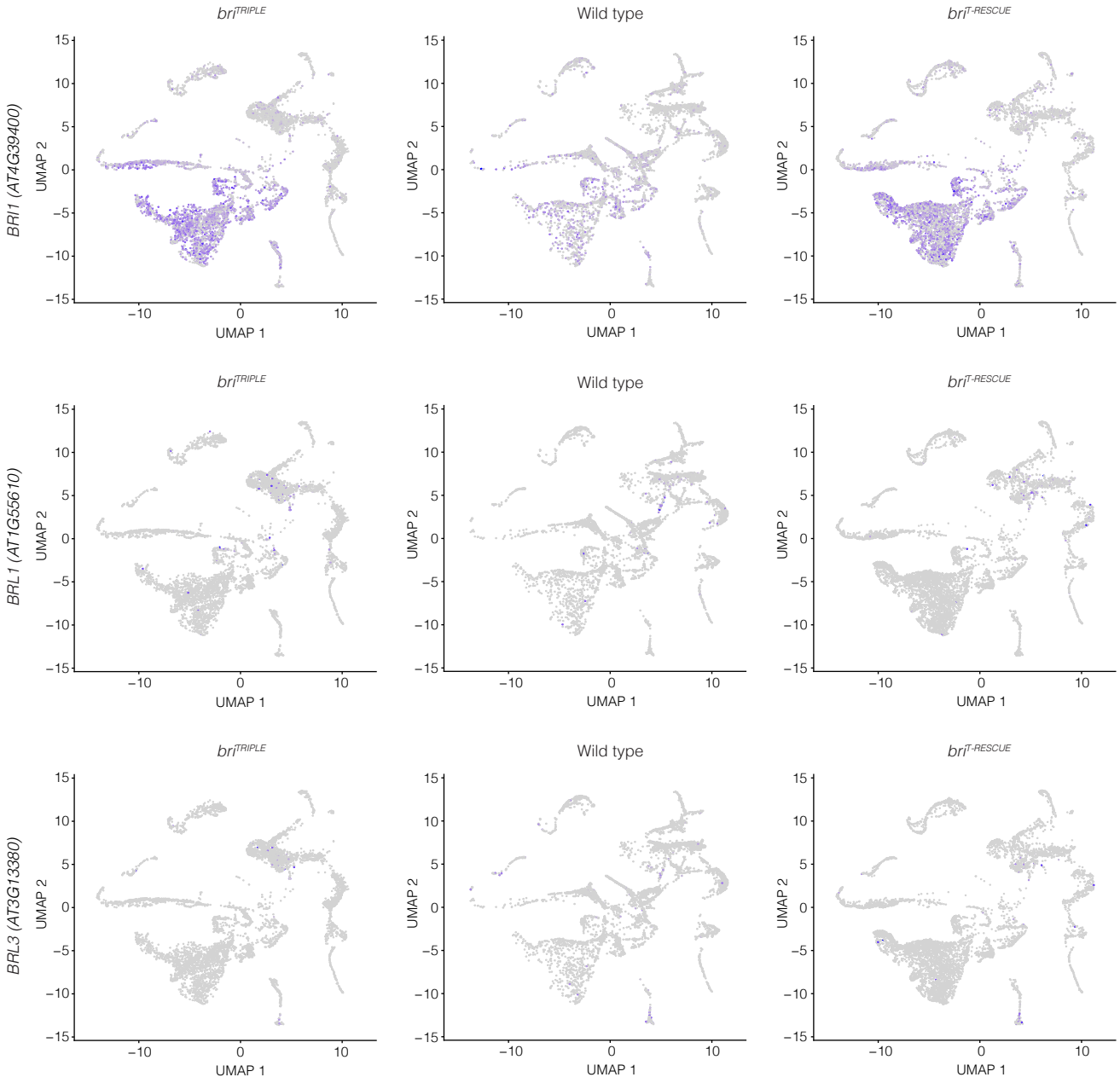

Figure S20 Brassinosteroid receptor gene expression in the scRNAseq profiles Feature plots of *BRI1*, *BRL1* and *BRL3* expression in the different genotypes. Note the overall low expression levels, and the presence of background mutant *BRI1* mRNA.

Graeff et al. 2021

Methods S1

Julien Dorier
Bioinformatics Competence Center, University of Lausanne

February 9, 2021

1 Description

1.1 Straightening & restoring radial symmetry

1.1.1 Input data

For each sample, a table exported from `MorphoGraphX` [1] with the following properties for each cell:

- Positions of cell centers $\{r_i = (x_i, y_i, z_i)\}$.
- Identity: Quiescent center cells should have identity "QC", a series of selected xylem cells perpendicular to the main axis should have identity "xylem_axis". Positions of these quiescent center and xylem axis cells will be used to perform initial alignment of the root.
- Volume, longitudinal length, radial length, circumferential length, ...: these properties will be used for visualization (e.g. size of spheres or ellipsoid) and will be aggregated and reported in the analysis section.

Cells satisfying any of the following properties are considered as outliers and ignored:

- $x_i \notin \left[P_5^{(x)} - 1.5\left(P_{95}^{(x)} - P_5^{(x)}\right), P_{95}^{(x)} + 1.5\left(P_{95}^{(x)} - P_5^{(x)}\right)\right]$
- $y_i \notin \left[P_5^{(y)} - 1.5\left(P_{95}^{(y)} - P_5^{(y)}\right), P_{95}^{(y)} + 1.5\left(P_{95}^{(y)} - P_5^{(y)}\right)\right]$
- $z_i \notin \left[P_5^{(z)} - 1.5\left(P_{95}^{(z)} - P_5^{(z)}\right), P_{95}^{(z)} + 1.5\left(P_{95}^{(z)} - P_5^{(z)}\right)\right]$

where $P_n^{(x)}$, $P_n^{(y)}$ and $P_n^{(z)}$ denote the n-th percentile of all $\{x_i\}$, $\{y_i\}$ and $\{z_i\}$ respectively.
For each sample, a mesh in Stanford ASCII ply format (optionally compressed with gzip).

1.1.2 Initial alignment

Let us denote by $\boldsymbol{Q}$ the centroid of the quiescent center cells (QC) and by $\boldsymbol{X}$ the centroid of the selected "xylem axis" cells. The xylem axis direction (denoted $\boldsymbol{v}$) is then obtained as the direction of largest variance[1] of the xylem axis cell centers projected onto the plane perpendicular to $\boldsymbol{X} - \boldsymbol{Q}$ (i.e. $\sim$ root axis direction). Finally, the unit vectors in direction x, y and z are denoted by $\boldsymbol{e}_x$, $\boldsymbol{e}_y$ and $\boldsymbol{e}_z$ respectively.
The following transformations are performed to align the root with the coordinate system:

- All cells are rotated to bring $\boldsymbol{X} - \boldsymbol{Q}$ parallel to $\boldsymbol{e}_z$ and v parallel to $\boldsymbol{e}_x$.
- All cell centers are translated by $-\boldsymbol{Q}$ to bring the quiescent center centroid to the origin.

Figure 1 shows cell centers after initial alignment.

[1] eigenvector of the covariance matrix corresponding to largest eigenvalue (could also be done with PCA).

1.1.3 Main axis estimation

The main axis of the root is evaluated using a sliding window weighted average (using cell volume as weight) along the z axis (figure 2a and b), with the n-th window is defined as

$$\{(x, y, z) \in \mathbb{R} | z \in [(n-1)w/2, (n+1)w/2)]\}$$

where $w = (\max(\{z_i\}) - \min(\{z_i\}))/4$ is the window width and $n = 1, 2, \cdots, 7$.
The main axis is then smoothed and extrapolated (it is extended by 20% on each side) using a fit to a cubic spline[2] (figure 2c).
The resulting main axis is then divided into 8 segments by choosing 9 equidistant points (denoted $\{p_1, p_2, \cdots, p_9\}$) on the axis (figure 3 left). For each point p_j (with $j = 2, 3, \cdots, 8$), the local distribution of cell centers is summarized by two vector $\boldsymbol{a}_1$ and $\boldsymbol{a}_2$ (principal axes) perpendicular to the main axis at p_j, obtained with the following procedure:

- Consider all cell centers lying between the planes (1) perpendicular to the main axis at p_{j-1} and passing through p_{j-1} and (2) perpendicular to the main axis at p_{j+1} and passing through p_{j+1}. Example: figure 3a, the selected region for p_6 is shown in light blue.
- Project the selected cell centers on the plane perpendicular to the main axis at p_j and passing through p_j.
- Evaluate eigenvectors ($\boldsymbol{v}_1, \boldsymbol{v}_2$ and $\boldsymbol{v}_3$) and eigenvalues ($\lambda_1 \geq \lambda_2 \geq \lambda_3 = 0$[3]) of the weighted (with cell volume as weight) covariance matrix of the projected cell centers.
- Choose vector $\boldsymbol{a}_1$ parallel to v_1 with length $\sqrt{\lambda_1}$ and vector $\boldsymbol{a}_2$ parallel to v_2 with length $\sqrt{\lambda_2}$ (figure 3b).

The principal axes are then smoothed using a fit to a cubic spline[4] weighted by total cell volume of cell centers used at each point $p_2, p_3, \cdots, p_8$ (figure 3c).

1.1.4 Straightening and restoring radial symmetry

The smoothed main axis is divided into 1000 segments by choosing 1001 equidistant points (denoted $\{p_1, p_2, \cdots, p_1001\}$). At each point p_j (with $j = 1, 3, \cdots, 1000$), consider all cell centers lying between the planes (1) perpendicular to the main axis at p_j and passing through p_j and (2) perpendicular to the main axis at p_{j+1} and passing through p_{j+1} (the selected region for p_j is illustrated by a light blue in figure 4a). Let $\boldsymbol{a}_1$ and $\boldsymbol{a}_2$ denote the principal axes at point p_j (figure 4b and f)). The following transformations are applied to all considered cell centers:

- Scaling from point p_j by a factor $f_1 = \sqrt{|\boldsymbol{a}_1| \cdot |\boldsymbol{a}_2|}/|\boldsymbol{a}_1|$ in direction $f_2 = \boldsymbol{a}_1$ and by a factor $\sqrt{|\boldsymbol{a}_1| \cdot |\boldsymbol{a}_2|}/|\boldsymbol{a}_2|$ in direction $\boldsymbol{a}_2$.
- Rotation to bring the main axis tangent parallel to $\boldsymbol{e}_z$
- Translation to bring p_j at position $d \cdot \boldsymbol{e}_z$, with d the signed distance between p_j and the point of the main axis with $z = 0$, measured along the main axis curve.

This operation is repeated for all p_j with $j = 1, 3, \cdots, 1000$.

1.1.5 Final alignment

After straightening and restoration of the radial symmetry, the main axis pass through the origin of the coordinate system. However, the centroid of the quiescent center cells is not necessarily exactly on the main axis and therefore not on the origin. In addition, the non-isotropic scaling might changes the orientation of the xylem axis, resulting in xylem axis not parallel to the xz plane anymore.
Therefore a final alignment is performed:

- All cells are rotated to bring v parallel to $\boldsymbol{e}_x$.
- All cell centers are translated by $-\boldsymbol{Q}$ to bring the quiescent center centroid to the origin.

As in section "initial alignment", $\boldsymbol{Q}$ denotes the centroid of the quiescent center cells and $\boldsymbol{v}$ denotes the xylem axis direction evaluated using cell centers after straightening and restoration of the radial symmetry.

[2] using R function `stats::smooth.spline()` with default parameters.
[3] due to the projection on the plane
[4] using R function `stats::smooth.spline()` with default parameters and `df=5`.

1.1.6 Mesh

Mesh vertices are transformed using the same transformations as the cell centers (i.e. initial alignment as well as local translation, rotation and scaling to straighten and restore radial symmetry and final alignment). The parameters of the transformations are estimated on the cell centers, but the resulting transformations are applied to all positions (cell centers and mesh vertices).
Each mesh is then smoothed using the following operations in `meshlab` [2] (version 2020.07):

- "Merge close vertices" (with default parameters).
- "Laplacian Smooth" (with default parameters).

1.2 Analysis

1.2.1 Cells data

Various cell properties are summarized using sliding windows along radial direction (r) and along the main axis direction z. In this analysis, original cell properties exported from `MorphoGraphX` are used (cell volume, cell wall area, longitudinal length, radial length and circumferential length). These properties are not transformed together with cell center positions when straightening and restoring radial symmetry. For this analysis, all cells from all sample in the group (genotype) are pooled together. Cells with volume below 10μm^3 or above 50000μm^3 are ignored.
Each window is a cylindrical shell (figure 5) defined as the set of points $(x, y, z) \in \mathbb{R}$ such that $z \in [z_{min}, z_{max})$ and $r\sqrt{x^2 + y^2} \in [r_{min}, r_{max})$.
For a given window, the distribution of a cell property (e.g. radial cell length) is summarized by evaluting the average and standard deviation over all cells with center[5] inside the window. The standard error of the mean (sem) is evaluated as (standard deviation)$/\sqrt{n}$ with n the number of cell centers inside the window. In the limit of large n, the sem can be used to estimate a 95% confidence interval for the average: [average-2*sem,average+2*sem].
In addition to sliding window averages of cell properties, the sliding window cell density per sample is evaluated as the total number of cell centers in each window divided by (volume of the window)*(number of samples in the group). Note that the cell density is measured after straightening and restoring radial symmetry.

Sliding windows along the radial direction: For a given z range $[z_{min}, z_{max})$, a window of size $\Delta r = 10\mu$m centered on r (i.e. with $r_{min} = r - \Delta r/2$ and $r_{max} = r + \Delta r/2$) is used to evaluate average and sem of a gvien cell property. This operation is repeated by placing the windows at regularly spaced r positions. As an example, the average radial cell length obtained with sliding windows with $z \in [250, 300)$ is shown in figure 6. Figure 7 shows an example of cell density for the same set of windows.

Sliding windows along the z direction: For a given r range $[r_{min}, r_{max})$, a window of size $\Delta z = 50\mu$m centered on z (i.e. with $z_{min} = z - \Delta z/2$ and $z_{max} = z + \Delta z/2$) is used to evaluate average and sem of a gvien cell property. This operation is repeated by placing the windows at regularly spaced z positions. As an example, the average radial cell length obtained with sliding windows with $r \in [20, 30)$ is shown in figure 8. Figure 9 shows an example of cell density for the same set of windows.

1.2.2 Meshes

The goal of this analysis is to estimate the distribution of triangle directions (weighted by triangle area) per unit of solid angle
Each mesh is first transformed using the same transformations as the corresponding cell centers (i.e. initial alignment as well as local translation, rotation and scaling to straighten and restore radial symmetry and final alignment).
Triangles with z coordinate of the centroid above 300μm or below 0μm are ignored.
Let us denote by $\boldsymbol{n}_i$ the unit vector perpendicular to the plane containing the i-th triangle of the mesh, and by A_i its area. $\boldsymbol{n}_i = (n_{i,x}, n_{i,y}, n_{i,z})$ can be expressed with spherical coordinates (figure 10)

$$\begin{aligned} n_{i,x} &= sin(\theta_i)cos(\varphi_i) \\ n_{i,y} &= sin(\theta_i)sin(\varphi_i) \\ n_{i,z} &= cos(\theta_i) \end{aligned}$$

To evaluate the distribution of triangle directions (i.e. $\{\boldsymbol{n}_i\}$), the spherical coordinates (θ and ϕ) are partitioned into bins of size $\Delta\theta = \Delta\varphi = \pi/200$.

[5] after straightening and restoring radial symmetry

For each triangle, the area A_i is assigned to the bin corresponding to its normal vector $\boldsymbol{n}_i$ falls. The area A_i is also assigned to the bin corresponding to the opposite vector $-\boldsymbol{n}_i$. The distribution of triangle directions is then obtained by summing all areas assigned to each bin, and normalizing by the bin area[6] (i.e. solid angle covered by the bin).
Note that with this normalization, an isotropic distribution of triangle directions will produce a flat distribution (same value for all bins).
The resulting distribution of triangle directions (weighted by triangle area) per unit of solid angle can be visualized on a sphere (figure 11), in the $\varphi\theta$ plane (figure 12) or in polar coordinates with θ as radial coordinate and φ as angular coordinate (figure 12).
To focus on the dependence on θ, one can integrate over φ, i.e. sum all area per unit of solid angle with a given θ (figure 14). Note that with the chosen normalization, an isotropic distribution of triangle directions will produce a flat distribution (same value for all bins).

2 Implementation

All methods were implemented in `R` [3], using the following packages

- `rgl` [4].
- `geomorph` [5].
- `data.table` [6].
- `ggplot2` [7].
- `cowplot` [8].

Meshes were smoothed using `meshlab` [2] (version 2020.07).

References

[1] P. B. de Reuille *et al.* (2015). *MorphoGraphX: A platform for quantifying morphogenesis in 4D*. eLife 4:e05864. https://www.mpipz.mpg.de/MorphoGraphX

[2] P. Cignoni *et al.* (2008) *MeshLab: an Open-Source Mesh Processing Tool*. Sixth Eurographics Italian Chapter Conference. https://www.meshlab.net/

[3] R Core Team (2020). *R: A language and environment for statistical computing*. R Foundation for Statistical Computing, Vienna, Austria. http://www.R-project.org/. R version 4.0.3.

[4] D. Adler, D. Murdoch *et al.* (2020). *rgl: 3D Visualization Using OpenGL*. R package version 0.103.5. https://CRAN.R-project.org/package=rgl

[5] D. C. Adams, M. L. Collyer and A. Kaliontzopoulou (2020). *Geomorph: Software for geometric morphometric analyses*. R package version 3.3.1. https://cran.r-project.org/package=geomorph

[6] M. Dowle and A. Srinivasan (2020). *data.table: Extension of 'data.frame'*. R package version 1.13.6. https://CRAN.R-project.org/package=data.table

[7] H. Wickham (2016). *ggplot2: Elegant Graphics for Data Analysis*. Springer-Verlag New York. R package version 3.3.3. https://ggplot2.tidyverse.org

[8] C. O. Wilke (2020). *cowplot: Streamlined Plot Theme and Plot Annotations for 'ggplot2'*. R package version 1.1.1. https://CRAN.R-project.org/package=cowplot

[6] $(\varphi_2 - \varphi_1)(cos(\theta_1) - cos(\theta_2))$ is the area of the bin $[\theta_1, \theta_2] \times [\varphi_1, \varphi_2]$.

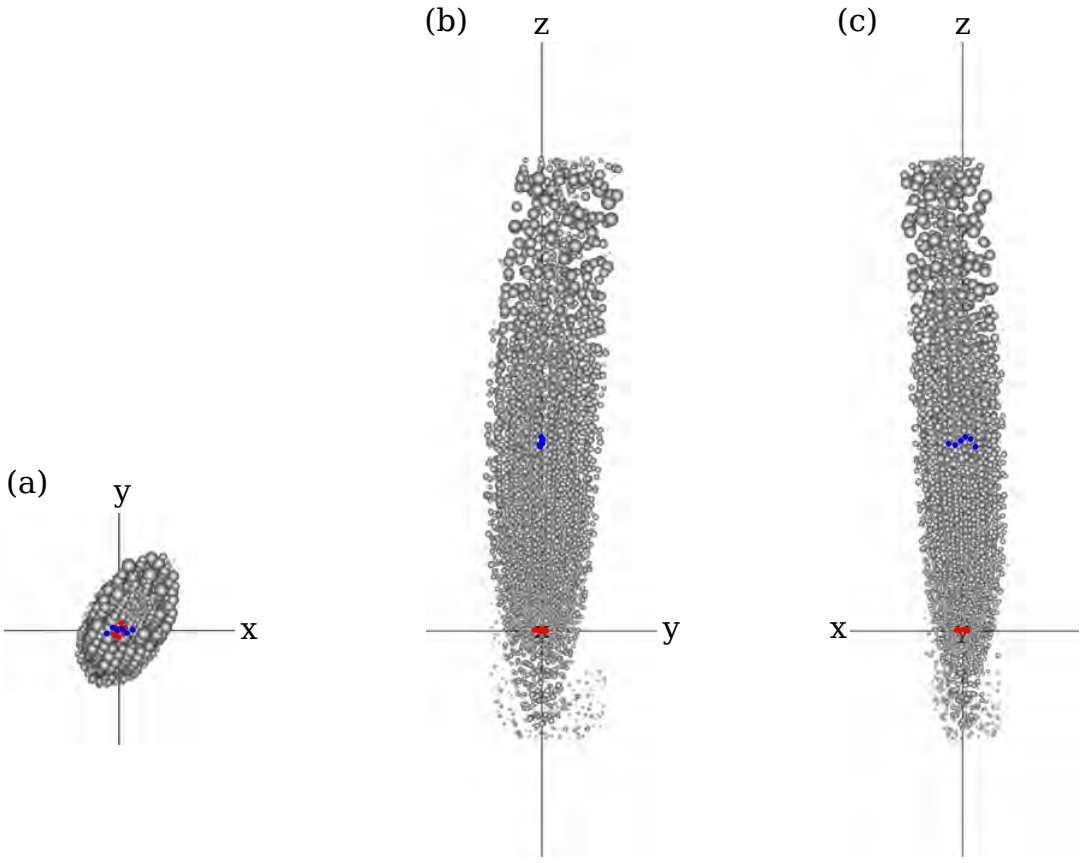

Figure 1: Cell centers after initial alignment. Cell centers are represented as spheres with volume proportional to cell volumes. Quiescent center cells (red) and selected xylem axis cells (blue) are shown with colored circles.

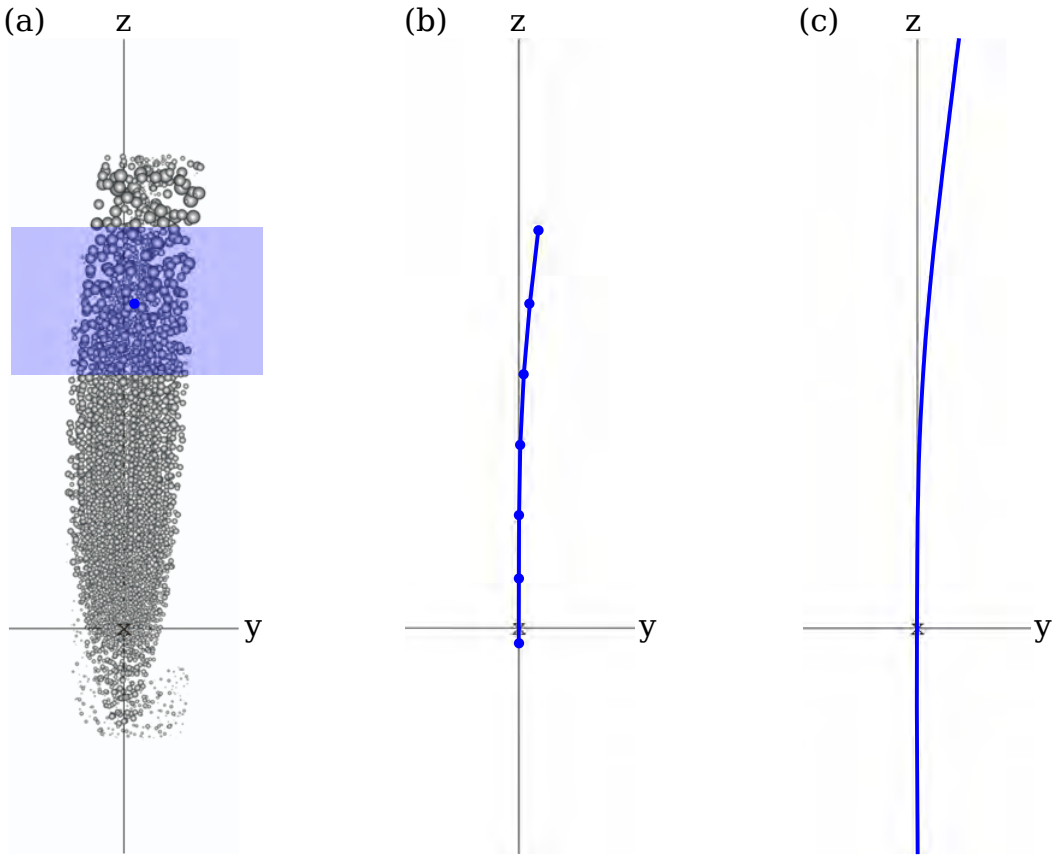

Figure 2: Main axis evaluation using sliding windows (a-b) and spline smoothing (c).

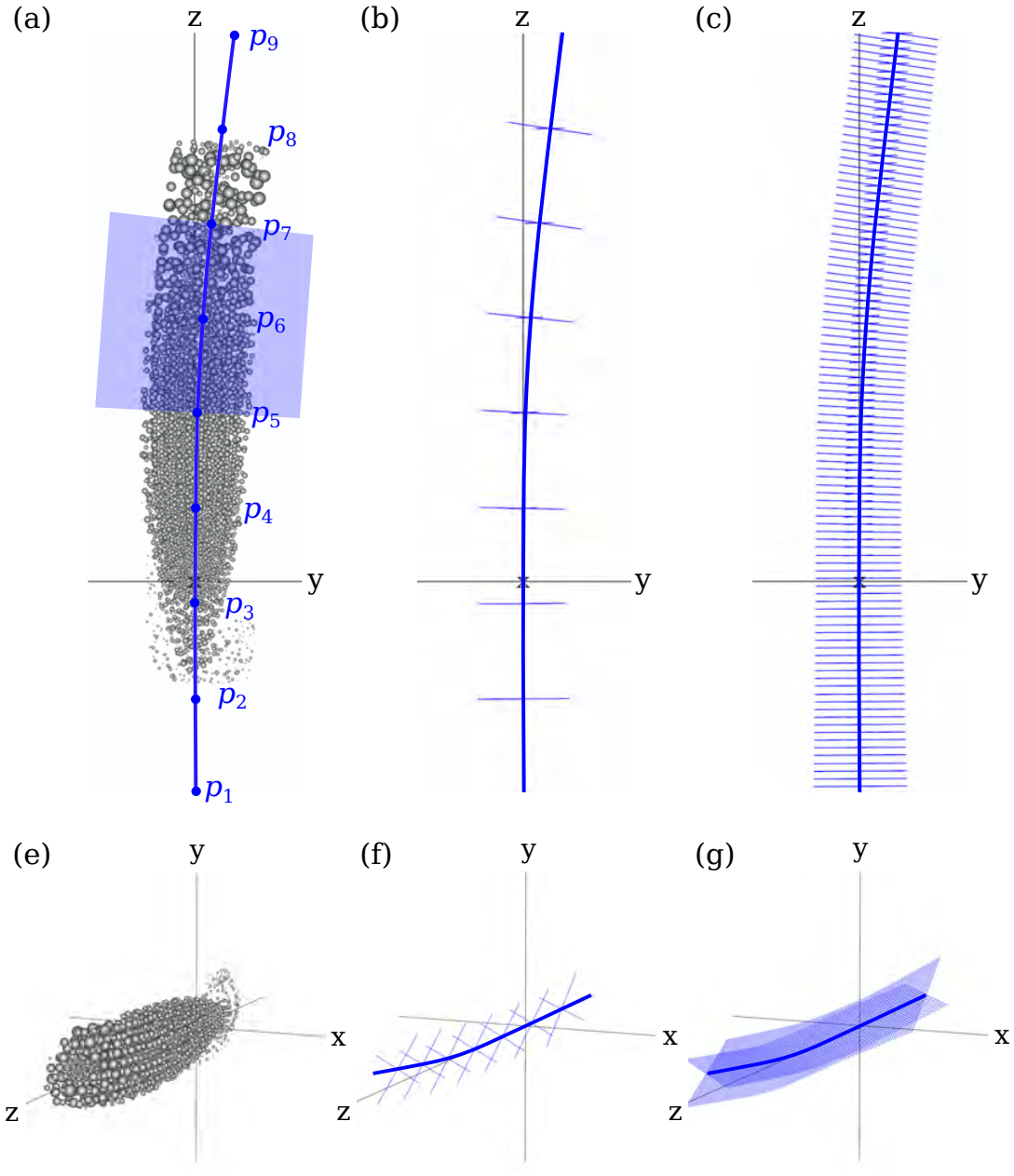

Figure 3: Evaluation of principal axes along the main axis (a-b and e-f) and spline smoothing (c and g). Top and bottom rows present the same plots with different view points.

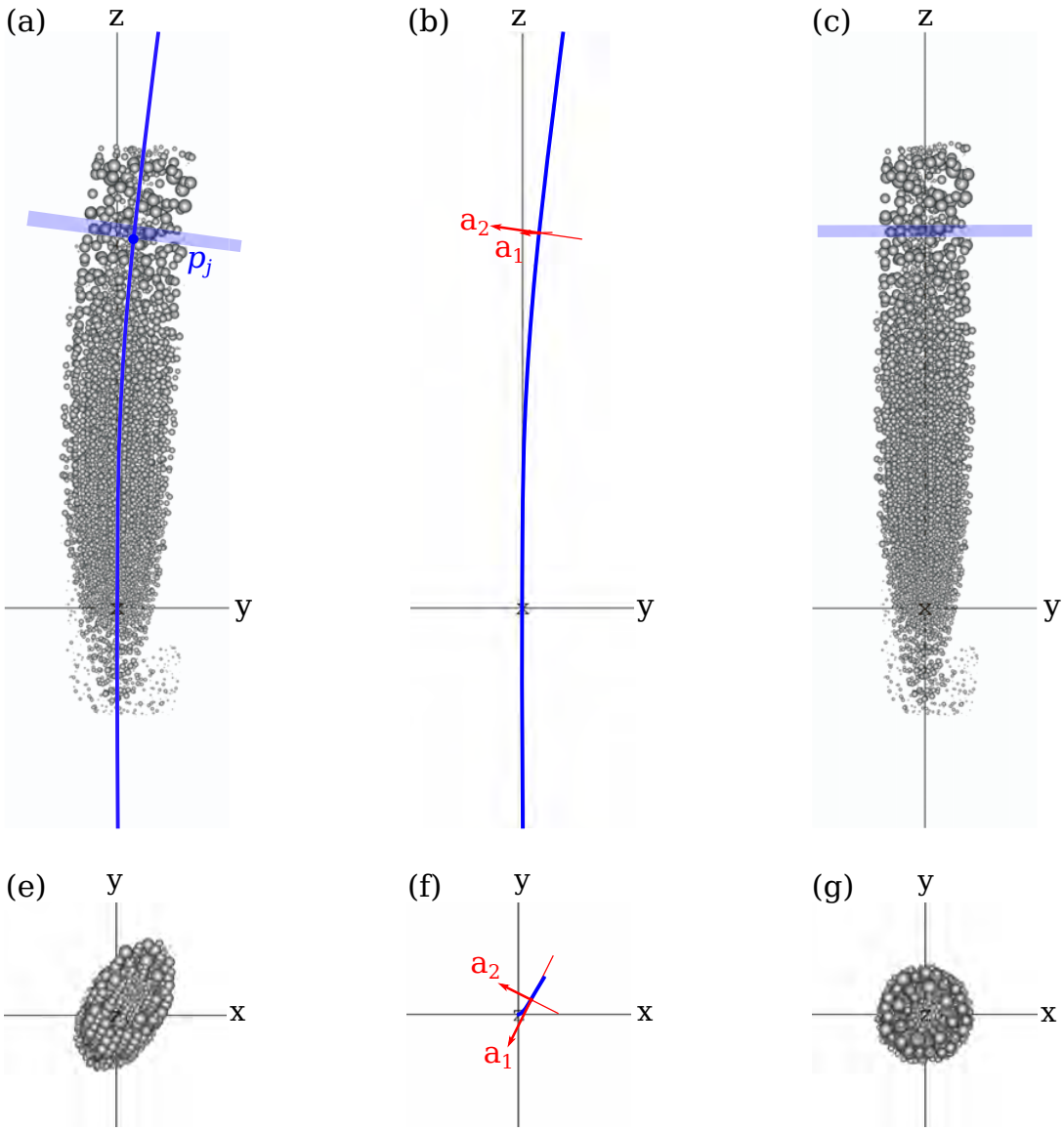

Figure 4: Cell centers after initial alignment (a,e) with selected region in light blue, main axis (blue) with principal axes (red) in the selected region (b,f). Cell centers after straightening and radial symmetry restoration (c,g).

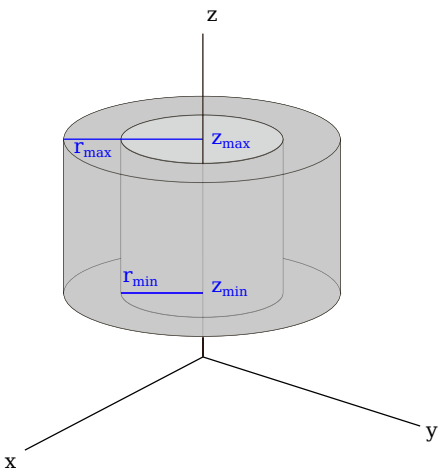

Figure 5: Cylindrical shell region.

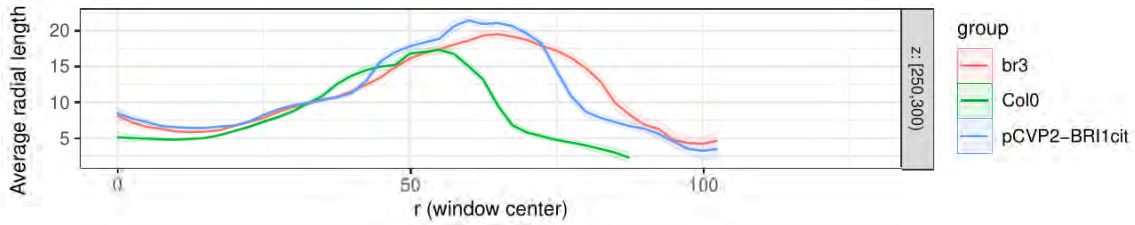

Figure 6: Average (colored lines) radial cell length versus radial position of the window, colored by group (genotype). Radial cell length, r and z are in μm. Shaded regions extend by ± 2(standard error of the mean) around the average and correspond approximately to the 95% confidence interval for the average. The standard error of the mean (sem) is obtained as (standard deviation)$/\sqrt{n}$, with n the number of cell centers inside the window.

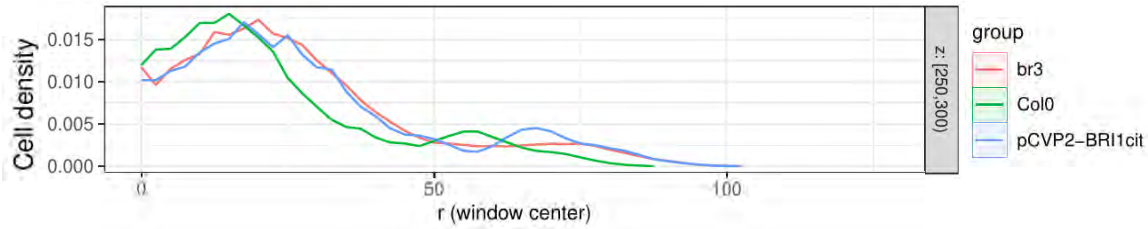

Figure 7: Cell density (number of cells/(window volume * number of samples in the group), in μm^{-3}) versus radial position of the window (μm), colored by group (genotype).

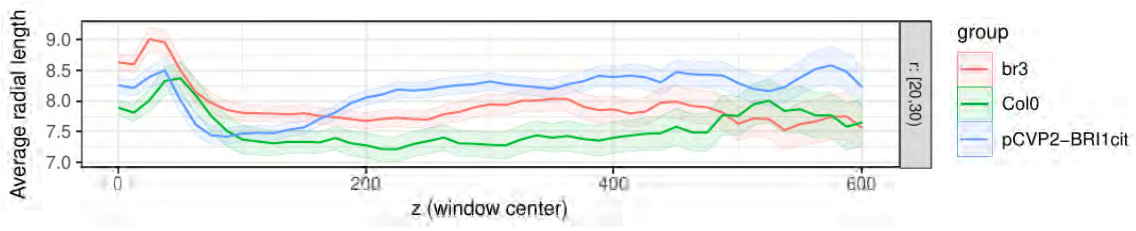

Figure 8: Average (colored lines) radial cell length versus z position of the window, colored by group (genotype). Radial cell length, r and z are in μm. Shaded regions extend by ± 2(standard error of the mean) around the average and correspond approximately to the 95% confidence interval for the average. The standard error of the mean (sem) is obtained as (standard deviation)$/\sqrt{n}$, with n the number of cell centers inside the window.

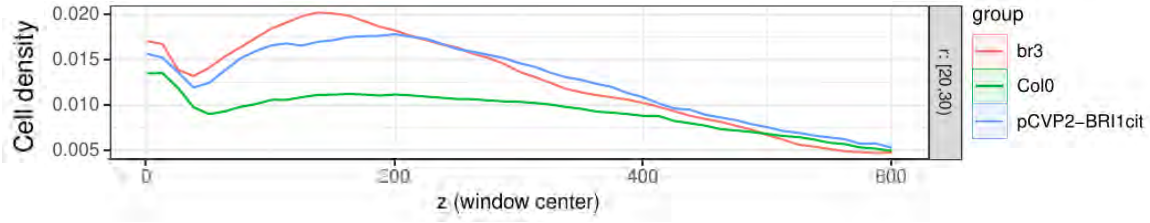

Figure 9: Cell density (number of cells/(window volume * number of samples in the group), in μm^{-3}) versus z position of the window (μm), colored by group (genotype).

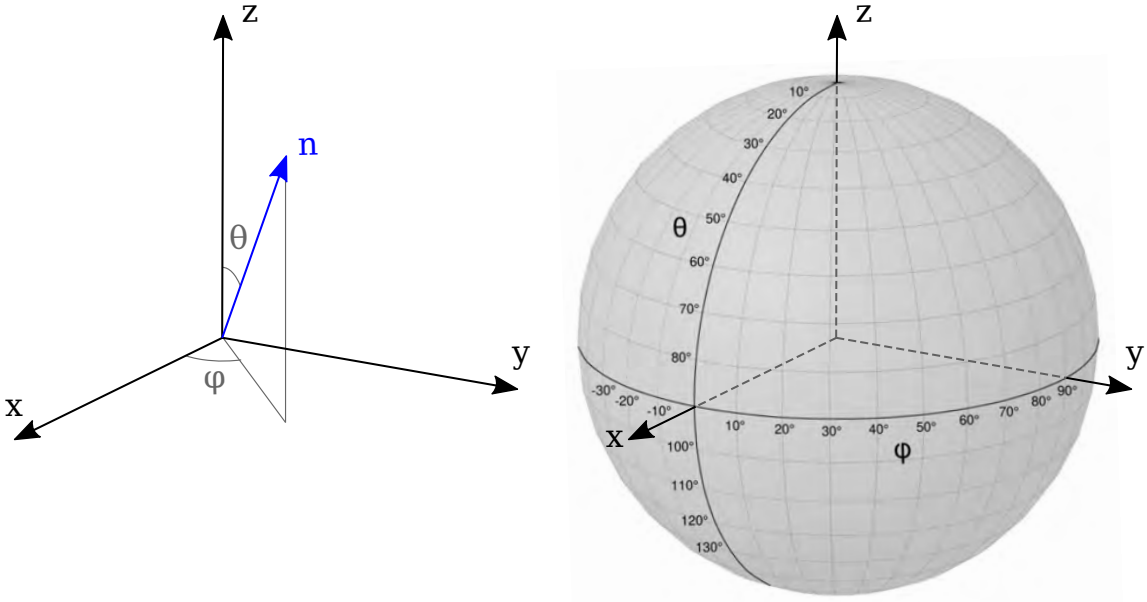

Figure 10: Spherical coordinates.

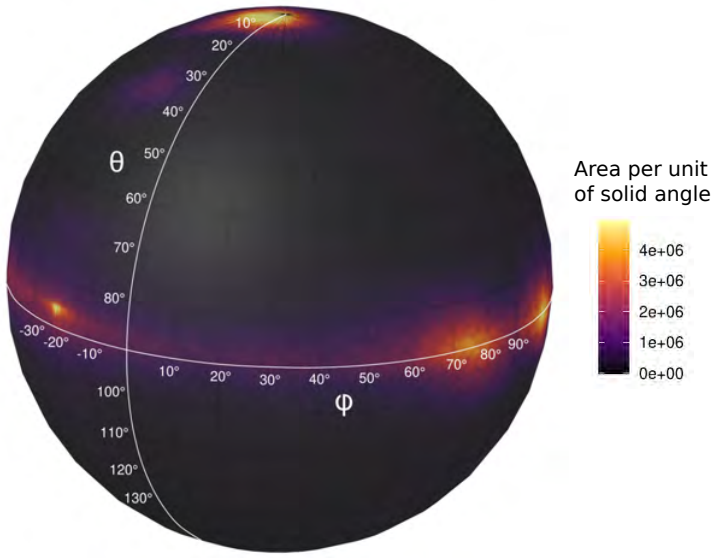

Figure 11: Distribution of triangle directions (weighted by triangle area) per unit of solid angle.

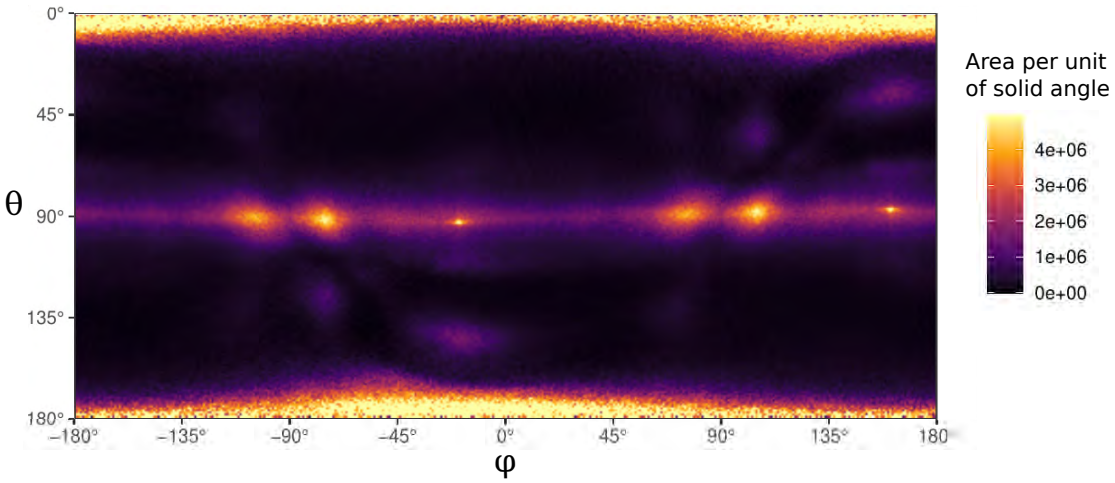

Figure 12: Distribution of triangle directions (weighted by triangle area) per unit of solid angle.

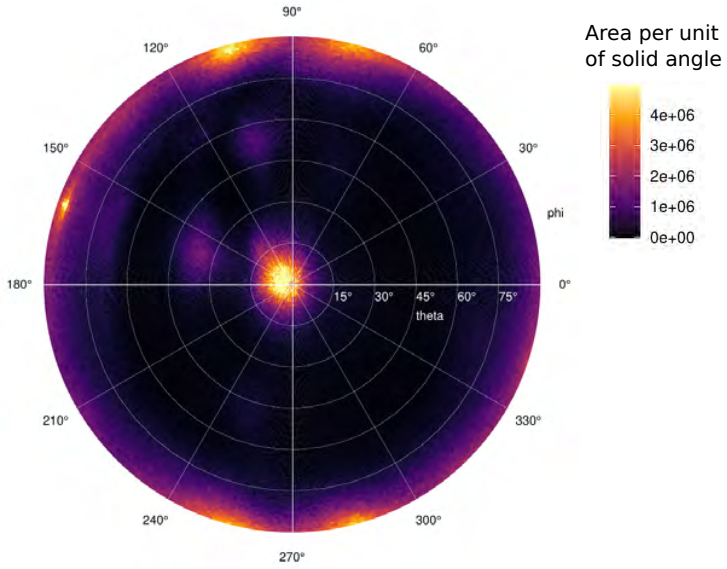

Figure 13: Distribution of triangle directions (weighted by triangle area) per unit of solid angle.

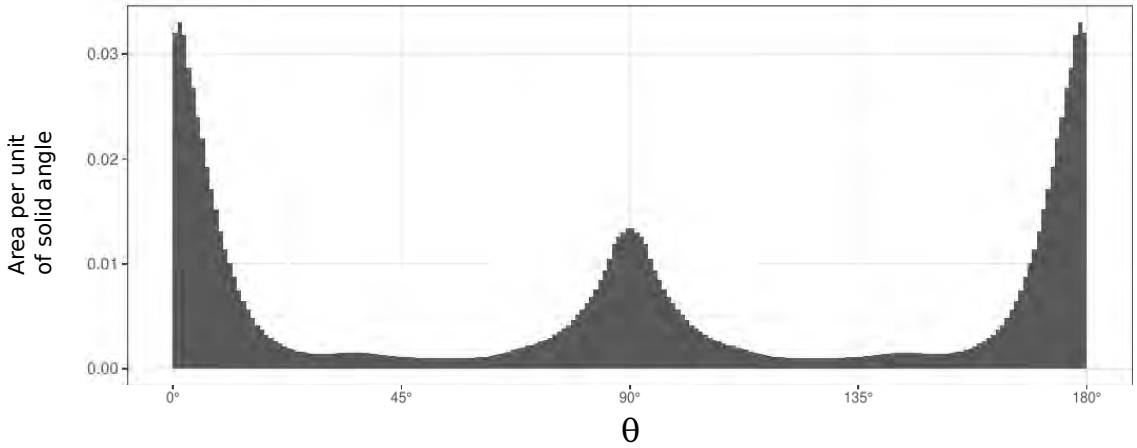

Figure 14: Distribution of triangle directions (weighted by triangle area) per unit of solid angle (sum over φ), normalized so as to have a total area of one.